SGG SGS sc | nat
Swiss Journal of Geosciences

ORIGINAL PAPER Open Access

The Val Biandino Intrusive Suite (central Southern Alps, N Italy): new geochronological and geochemical data on the Early Permian magmatic activity in the Southalpine Domain

Stefano Zanchetta[1*], Chiara Crippa[1], Andrea Zanchi[1] and Chiara Montemagni[1]

Abstract

The Early Permian in the present-day Europe area was a time when a major tectonic shift occurred, leading from the tectonic collapse of the Variscan orogeny to the crustal extension and thinning that characterized the Early Permian times. Crustal extension was associated with extensive magmatism at different crustal levels: from gabbro in the lower crust or at the mantle/crust transition to subaerial high-SiO_2 volcanic activity. In the whole Southalpine Domain, the Early Permian intrusive bodies occur from the west (e.g. Ivrea-Verbano Complex and "Graniti dei Laghi") to the east (Ifinger, Brixen and Cima d'Asta intrusive complexes). Among these, in the central Southern Alps (comprised between the Giudicarie Belt and the Lake Como), minor intrusive complexes also occur. The Val Biandino Intrusive Suite consists of two magmatic units: the Val Biandino Quartz-Diorite (VBQD) and the Valle di San Biagio Granite (VSBG). The first of them consists of gabbro-diorite to granodiorite bodies associated with leucocratic cordierite-bearing granitic dikes that intruded the pre-Permian basement. To the west, a W-dipping normal fault of Permian age represents the boundary between this unit and the Valle di San Biagio porphyric granite. All rock varieties of the Val Biandino Intrusive Suite display a high-K calc-alkaline affinity with metaluminous to peraluminous character. Field crosscutting relationships point to a late generation of the cordierite granites of the Val Biandino Quartz-Diorite unit with respect to the more mafic types. SHRIMP U–Pb zircon dating provided an age of 285.2 ± 1.9 Ma for a cordierite granite of the Val Biandino Quartz-Diorite unit and 283.2 ± 1.9 Ma for the porphyric Valle di San Biagio Granite. Geochemical data suggest that gabbro-diorite, quartz-diorite, granodiorite and leucogranite are not co-magmatic. The existing gaps in term of SiO_2 wt% and the higher HREE contents in mafic and intermediate rocks with respect to granite coupled with similar LREE in all rocks support this hypothesis. The high Rb/Sr ratios (> 1) in leucogranite, together with the occurrence of white mica and cordierite point to a significant contribution of crustal partial melting in their genesis. The Val Biandino Intrusive Suite was likely formed through the interaction of magma genesis at the mantle/crust transition and partial melting of the heterogeneous pre-Permian basement of the Southalpine Domain. This scenario explains the strong heterogeneity displayed by the relatively small intrusive complex and the strong crustal signature exhibited by all the magmatic types of the Val Biandino Intrusive Suite.

Keywords Early Permian magmatism, Rifting, Cordierite granite, Crustal melting

Editorial handling: Paola Manzotti

*Correspondence:
Stefano Zanchetta
stefano.zanchetta@unimib.it
Full list of author information is available at the end of the article

1 Introduction

During Late Carboniferous to Early Permian times, the Variscan orogenesis faced end and subsequent tectonic collapse of the orogen. The kind of geodynamic model that actually led to the break-up of Pangea and the formation of intracontinental Permian basins accompanied by magmatic activity in the present-day Europe area is still largely debated (e.g. Ménard & Molnar, 1988; Echtler & Malavieille, 1990; Burg et al., 1994; Rottura et al., 1998; Cagnard et al., 2004; Casini & Oggiano, 2008; Le Pichon et al., 2019, 2021; Fréville et al., 2022). Several mechanisms have been proposed to be responsible for the Early Permian phase of crustal extension and lithospheric thinning. Many interpretations cluster around three hypotheses: (i) a tectonic regime characterized by dextral transtension (e.g. Arthaud & Matte, 1977; Cassinis & Perotti, 1994) and wrenching associated to the transition from Pangea A to Pangea B configuration (Muttoni et al., 2003; Schaltegger & Brack, 2007; Pohl et al., 2018), (ii) an orogenic collapse stage (Dewey, 1988; Ménard & Molnar, 1988; Malavieille et al., 1990; Malavieille, 1993) at the end of the Variscan orogenesis, accompanied by almost pure N-S directed extension (in the present-day coordinates), (iii) lithospheric extension and thinning at the initial stage of continental rifting (Lardeaux & Spalla, 1991; Siletto et al., 1993). Several fault-controlled intracontinental basins of Late Carboniferous to Late Permian age are preserved to the north of the present-day Alps belt (e.g. von Raumer, 1998; McCann et al., 2006), in the Southalpine Domain (e.g. Cadel et al., 1996; Cassinis et al., 2012; Berra et al., 2016; Zanchi et al., 2019; Locchi et al., 2022), but also within the axial belt of the Eastern and Western Alps (e.g. Capuzzo & Wetzel, 2004; Veselá et al., 2008).

The formation of intra-continental basins occurred together with a diffuse magmatic activity, recorded as emplacement of gabbro to gabbro-diorite bodies close to the lower crust–mantle transition (Sinigoi et al., 1991; Zingg et al., 1990; Tribuzio et al., 1999; Müntener et al., 2000; Rebay & Spalla, 2001), emplacement of intermediate to acidic intrusive complexes at mid to shallow crustal levels (e.g. Rottura et al., 1998; Steck et al., 2013; Bergomi et al., 2017; Boscaini et al., 2020) and volcanic activity at the surface, within or in the proximity of the intra-continental basins (Cadel et al., 1996; Cortesogno et al., 1998; Schaltegger & Brack, 2007; Cassinis et al., 2012; Willcock et al., 2013).

Geochemical and geochronological studies of the Late Carboniferous—Early Permian magmatic activity in the Alps have been mainly focused on the gabbroic bodies within the Austroalpine and Penninic domains north of the Periadriatic Fault (e.g. Rebay & Spalla, 2001; Spalla et al., 2014; Manzotti et al., 2015; Petri et al., 2017; Bergomi et al., 2017; Ballèvre et al., 2020 with references), where original field relationships between magmatic-volcanic rocks and hosting metamorphic/sedimentary rocks have been severely overprinted by Alpine deformation and metamorphism.

In the Southalpine Domain deformation and metamorphism related to the Alpine collision were much less severe and allow to a valuable reconstruction of the architecture and stratigraphic evolution of the Permian basins and volcanic units, together with the intrusive relationships and the thermal aureole associated to magmatic bodies (e.g. Wyhlidal et al., 2012). Most of available data however cluster in the western (i.e. Ivrea-Verbano Zone; Sinigoi et al., 1991; Schaltegger & Brack, 2007) and eastern sectors (Marocchi et al., 2008; Bargossi et al., 2010; Boscaini et al., 2020) of the Southalpine Domain (Fig. 1), with the central Southern Alps (CSA) that appear to be under-investigated. Geochronological and geochemical data are limited to the volcanics occurring in the Laghi Gemelli Group (Brack & Schaltegger, 1999; Schaltegger & Brack, 2007; Gretter et al., 2013; Berra et al., 2015), on the intrusive bodies of the Val Trompia area (Locchi, 2023) and to the Val Biandino Intrusive Suite (Pohl et al., 2018). Even if geochronological data obtained from high-retentivity geochronometers (e.g. U–Pb on zircon) are available for the Val Biandino Intrusive Suite, no complete geochemical datasets considering all major and trace elements commonly used to decipher the petrogenesis and evolution magmatic complexes (De Capitani & Liborio, 1988; De Capitani et al., 1994) are available.

In this work we provide, based on new geochemical and geochronological data, insights on the magmatic evolution of the Val Biandino Intrusive Suite. We show how, despite its small size, the study of the Val Biandino Intrusive Suite could help in the understanding of the Early Permian magmatism in the Southalpine Domain. The fact that intermediate and felsic plutons that were emplaced at different crustal levels crop out in a relative small area allow to investigate their genetic relationships, shading some lights on the mechanisms of magma genesis and evolution of the magmatic systems during the Early Permian extensional phase in southern Europe.

2 Geological setting

The Val Biandino Intrusive Suite (Pohl et al., 2018) crops out in the central sector of the Southalpine Domain (central Southern Alps, CSA in Fig. 1), defined as the area comprised between Lake Como and the Giudicarie Fault System. The CSA are a thick-skinned fold-and-thrust belt that extends from the Periadriatic Fault to the north, active at least since the Oligocene (Schmid et al., 1989; Zanchetta et al., 2023), and the Po plain to the south. In the CSA, sedimentary and magmatic rocks of Permian

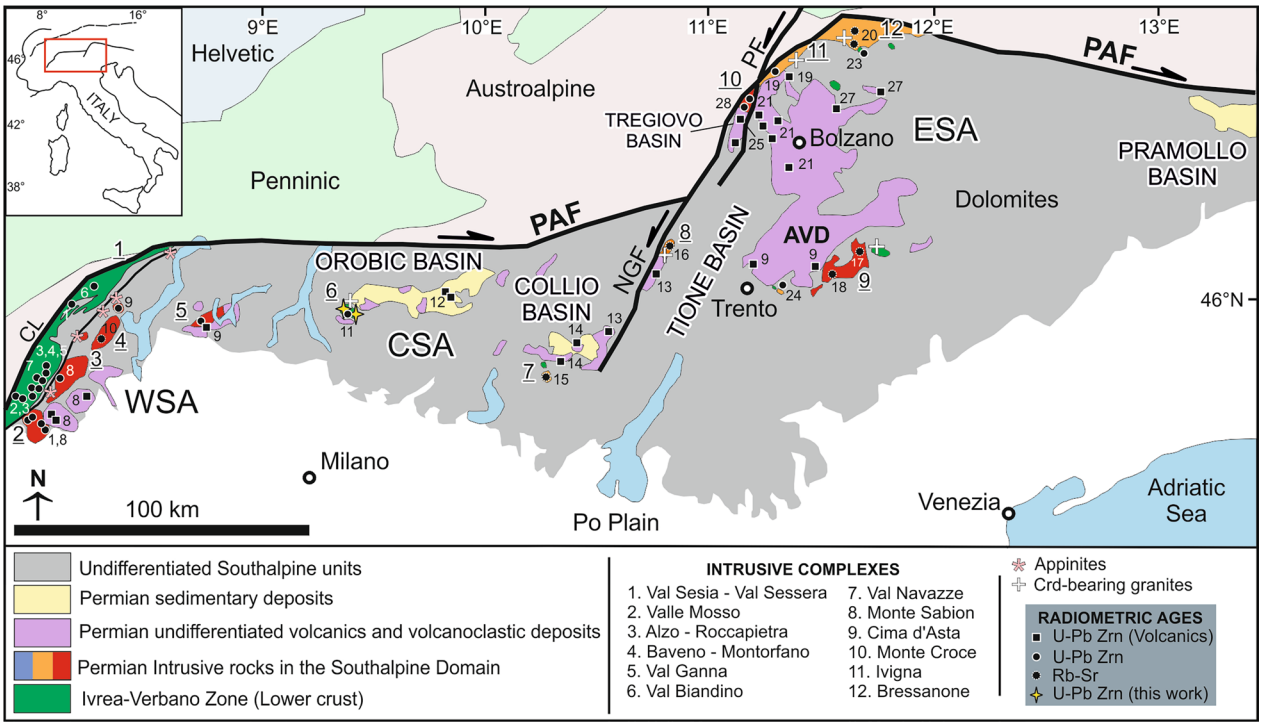

Fig. 1 Tectonic scheme of the Alps with highlighted all the occurrences of Permian volcanic and intrusive rocks. Small number in black refer to references reported in Table SUPP1 (age compilation of volcanic and intrusive rocks in the Southalpine Domain) and below. Only ages obtained from high-retentivity isotopic system have been preferred where available for each magmatic complex. CSA: central Southern Alps; ESA: eastern Southern Alps; WSA: western Southern Alps. [1] Klötzli et al., 2014; [2] Sinigoi et al., 2011; [3] Peressini et al., 2007; [4] Quick et al., 2003; [5] Garuti et al., 2001; [6] Vavra et al., 1999; [7] Pin, 1986; [8] Quick et al., 2009; [9] Schaltegger & Brack, 2007; [10] Pinarelli et al, 1988; [11] Pohl et al., 2018; [12] Berra et al., 2015; [13] Gretter et al., 2013; [14] Brack & Schaltegger, 1999; [15] De Capitani et al., 1994; [16] Borsi et al., 1966; [17] Macera et al., 1994; [18] Barth et al., 1994; [19] Morelli et al., 2012; [20] Rottura et al., 1998; [21] Marocchi et al., 2008; [22] Del Moro & Visonà, 1982; [23] Boscaini et al., 2020; [24] Avanzini et al., 2010; [25] Bargossi et al., 2010; [26] Piccin et al., 2009; [27] Visonà et al., 2007; [28] Klötzli et al., 2003

age are chiefly exposed at the core of three regional anticlines, called the Orobic Anticlines (De Sitter & De Sitter-Koomans, 1949; Schönborn, 1992). These anticlines occur just to the south of the Orobic-Porcile-Gallinera thrust system, a regional scale structure along which the Variscan basement was thrust over the Upper Pennsylvanian to Lower Triassic volcano-sedimentary cover (Laubscher, 1985; Schönborn, 1992; Blom & Passchier, 1997; Carminati et al., 1997; Zanchetta et al., 2011; D'Adda & Zanchetta, 2015; Zanchetta et al., 2015; Mittempergher et al., 2021). To the south of the Orobic Anticlines and the Adamello batholith (Fig. 1) another regional anticline occurs, the Monte Alto anticline (Schönborn, 1992). This regional-scale fold is responsible for the exposure of the Permian rocks below the Triassic and younger successions of the CSA (Fig. 1).

Despite the locally intense Alpine deformation that affected the Upper Pennsylvanian to Lower Triassic rocks of these anticlines, two distinct basins have been reconstructed: the Orobic Basin, corresponding to the three Orobic Anticlines, and the Collio Basin (or Val Trompia basin), corresponding to the Monte Alto anticline (Cassinis et al., 2007, Cassinis et al., 2012). Another small basin has been identified to the NW of the Collio one: the Boario Basin (Fig. 1; Cassinis et al., 2012). These basins developed from the Early Permian as fault-controlled basins (Zanchi et al., 2019; Locchi et al., 2022) in an extensional continental setting. Large amounts of volcanic products and siliciclastic sediments with thickness in the order of a few kilometres were accumulated (De Sitter & De Sitter-Koomans, 1949; Casati & Gnaccolini, 1967; Cassinis et al., 1988; Cadel et al., 1996; Berra & Carminati, 2010; Berra et al., 2016). Significant differences exist among the basins in terms of architecture, stratigraphic evolution and volcanic vs. siliciclastic prevalence (e.g. Cassinis et al., 2012).

The Val Biandino Intrusive Suite occurs at the western end of the Orobic Basin, that extends in a E-W direction for about 45 km, with a present width of less than 10 km (measured N-S). The oldest sediments deposited above the exposed Variscan basement, which forms the sole of the Orobic Basin, are fluvial conglomerates

(Conglomerato Basale, late Pennsylvanian?) with sandy matrix and clasts consisting of polycrystalline quartz and rare metamorphic clasts (Casati & Gnaccolini, 1967; Cadel et al., 1996). Above this unit that irregularly covers the metamorphic basement, the Permian succession starts with the Cabianca Volcanite (the Lower Collio Fm. *Auctorum*) consisting of pyroclastic flows, tuffs and minor terrigenous deposits and continues with mainly siliciclastic sediments with rare tuffs of the Pizzo del Diavolo Fm. (Upper Collio *Auctorum*) (Berra & Felletti, 2010; Gaetani et al., 2012; Berra et al., 2016). The Pizzo del Diavolo Fm., the Cabianca Volcanite and the Conglomerato Basale are grouped together in the Laghi Gemelli Group (Berra et al., 2016).

In the Valsassina area the total thickness of the Permian succession is about 1200 m (Gaetani et al., 1986; Sciunnach, 2003). The end of the Permian cycle is marked by a gap during the Middle Permian, followed by the deposition of red fluvial conglomerates of the Lopingian Verrucano Lombardo, that rest with an angular unconformity above the Pizzo del Diavolo Fm. (Gaetani et al., 1986; Sciunnach, 2001a). The thickness of the Verrucano Lombardo displays significant lateral variations, testifying for the occurrence of a complex paleo-topography, likely controlled by active tectonics possibly due to a partial inversion of the Cisuralian basins (Sciunnach, 2003), at the end of the pre-Verrucano Permian volcano-sedimentary cycle. In the western part of the Orobic Anticline the Laghi Gemelli Group is overlying a metamorphic basement made of quartz-rich two-mica gneiss (referred in the literature as the Morbegno Gneiss, Cornelius, 1916) with minor micaschists, quartzites and amphibolites (Froitzheim et al., 2008).

2.1 The Val Biandino Intrusive Suite

The basement of the Valsassina area, at the western end of the central Southern Alps, was deformed and metamorphosed during the Variscan orogeny (e.g. Siletto et al., 1993). During the Early Permian, several magmatic bodies ranging from granitic to dioritic in composition (Pasquarè, 1967; De Capitani, 1982), often accompanied by several leucogranitic and aplitic dikes, intruded the hosting basement rocks. The Val Biandino Intrusive Suite has been subdivided in two distinct intrusive suites: the "Val Biandino pluton" and the "Valle di San Biagio Granite" (Porro, 1897; Crommelin, 1932; De Sitter & De Sitter-Koomans, 1949; Pasquarè, 1967). The Val Biandino pluton, here referred as the VBQD ("Val Biandino Quartz-Diorite" of Pohl et al., 2018) consists of four major bodies (Fig. 2). In addition to these major bodies, small stocks and lenses also occur (Fig. 2). The pink-colored porphyric "Valle di San

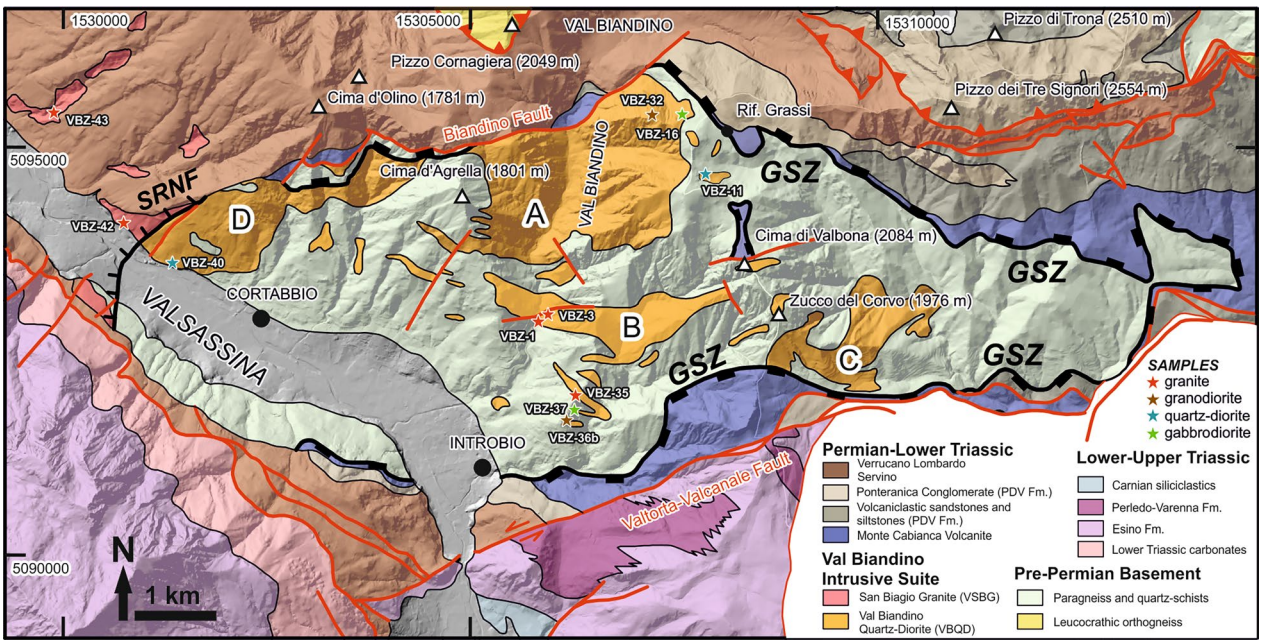

Fig. 2 Simplified geological map of the Valsassina northern sector. The Val Biandino Intrusive Suite is divided into two units: the "Val Biandino Quartz-Diorite" (VBQD) and the "Valle di San Biagio Granite" (VSBG). The VBQD crops out in a tectonic window bounded by the Grassi Shear Zone (GSZ; Froitzheim et al., 2008) and the Sassi Rossi Normal Fault (SRNF; Sciunnach, 2001b) intruding the late Variscan metamorphic basement of the central Southern Alps. The VSBG crops out in small erosional windows to the NW of the SRNF, below the Lopingian Permian Verrucano Lombardo. Analysed samples are reported in the map. A, B, C, and D are the four major stocks of the VBQD

Biagio Granite" (VSBG of Pohl et al., 2018), located to the NW of the Biandino pluton, is exposed in four erosional windows (Fig. 2) beneath the Southalpine sedimentary cover, here made by the continental deposits of the Verrucano Lombardo and the marly sandstones of the Servino (Gaetani et al., 1986).

The magmatic rocks of the VBQD, and their hosting paragneiss of the Southalpine basement, crop out in an area that extends in a E-W direction for about 15 km with a N-S maximum width of 7–8 km (Fig. 2). The contact between the basement with the overlying sedimentary-volcanic cover is tectonic and has been interpreted to represents a syn-magmatic detachment fault, the Grassi Detachment (Froitzheim et al., 2008; Pohl et al., 2018), that was responsible for the exhumation of the crystalline basement as a metamorphic core complex. The contact between the VBQD and the VSBG is tectonic and occurs along a NW-dipping high-angle tourmalinite-bearing normal fault (Fig. 2), the Sassi Rossi Fault (Sciunnach, 2001b; Pohl et al., 2018; Locchi 2023). This fault is crosscut atop by the erosional unconformity on which the Verrucano Lombardo conglomerates and sandstones deposited, directly above the Lower Permian rocks exposed at the surface during the Late Permian.

The main intrusive body of the VBQD crops out in the medium tract of the Biandino valley (A in Fig. 2, following the nomenclature of De Capitani & Liborio, 1988) and is made mainly of quartz-diorite accompanied by minor granite lenses and dikes. The second major body (B in Fig. 2) consists of tonalite and gabbro-diorite with granite lenses and dikes concentrated at its rims. Quartz-diorite and gabbro-diorite prevail in the Zucco del Corvo stock (C in Fig. 2), where the occurrence of gabbro have also been reported (Pasquarè, 1967). The westermost body crops out N of Cortabbio (D in Fig. 2) and consists almost exclusively of granodiorite, with some occurrence of fine-grained leucogranitic dikes at its southern rim.

Geochemical data (De Capitani, 1982; De Capitani & Liborio, 1988; De Capitani et al., 1994) indicate that rocks of the VBQD have a typical high-K calc-alkaline affinity and can be divided into two groups, based on the existence of a gap in the silica content. The first group represents the main part of the intrusive bodies, having a SiO_2 content lower than 64 wt%, whereas rocks of the other group, with SiO_2 higher than 68 wt%, occur as minor lenses and dikes of granitic composition at the rims of larger bodies.

The VSBG granite occurs NW of the VBQD, separated from this by the Sassi Rossi Normal Fault (Sciunnach et al., 2001b; SRNF in Fig. 2). The granite usually displays a pink color in the field with a porphyric to granophyric texture (Porro, 1897; De Sitter & De Sitter-Koomans, 1949).

Available K–Ar (De Capitani et al., 1988) and Rb–Sr (Thöni et al., 1992) whole rock and single mineral ages loosely constrain an intrusion age of 312 ± 48 Ma for the quartz-diorites and tonalities, i.e. the main intrusive bodies. More recent U–Pb LA-ICP-MS zircon data indicate a crystallization age of 289.1 ± 4.5 Ma for the VBQD and 286.8 ± 4.9 Ma for the VSBG (Pohl et al., 2018).

3 Methods

3.1 Whole rock geochemical analysis

The whole rock contents of major, minor and trace elements were determined at the ACME analytical labs, Vancouver (Canada). At least 500 g of fresh un-weathered material for each sample was crushed and pulverized. After quartering an amount of 20 g was used for analysis.

Total abundances of the major oxides were obtained by ICP-ES (Inductively Coupled Plasma Emission Spectroscopy), whereas REE (Rare Earth Element), refractory elements and precious and base metals by ICP-MS (Inductively Coupled Plasma Mass Spectroscopy). Samples were prepared for the ICP-MS analysis by a $LiBO_2$ fusion and dilute nitric digestion for major oxides, REE and refractory elements, whereas precious and base metals were digested in *aqua regia*. Analytical errors are within 2% for major elements and in the 5–10% range for trace elements, as determined by repeated analysis of the same sample (1 among 5).

3.2 U-Th-Pb dating of zircons

Two samples, a porphyric granite from the VSBG (VBZ43), and one quartz-diorite from the VBQD (VBZ3) were selected for U–Pb zircon dating. Samples were crushed, sieved and separated in two granulometric fractions (125–250 and 250–500 μm). The granulometric fractions were selected following thin section analyses that highlighted that most of the zircon grains population fall within those ranges. Zircon grains were concentrated by Wilfley table, heavy liquids and Frantz magnetic separator. Individual grains were hand-picked, ultrasonically cleaned in de-ionized water, and cast on a 3.5 cm diameter epoxy mount. The mount was then polished and documented at the optical microscope (reflected and transmitted light) and the scanning electron microscope (back-scattered and cathodoluminescence). After cleaning and drying, the mount was gold-coated. Zircon grains were analyzed by a sensitive high-resolution ion probe (SHRIMP) at the IBERSIMS laboratory, Granada University (Spain).

Each analytical spot was rastered with the primary ion beam ($^{16}O^{16}O^{+}$) for 120 s before analysis, the following isotopes were then measured: $^{196}Zr_2O$, ^{204}Pb, $^{204.1}$background, ^{206}Pb, ^{207}Pb, ^{208}Pb, ^{238}U, ^{248}ThO, ^{254}UO. The spot

diameter on mount was ca. 18 μm. The SL13 reference zircon (U: 210 ppm, Black et al., 2004) was used as standard for U concentrations. U/Pb ratios were calibrated using the TEMORA-II reference zircon (417 ± 1 Ma, Black et al., 2003). Common lead (^{204}Pb) was corrected from the measured ^{204}Pb/^{206}Pb using the model of terrestrial evolution of Pb of Cumming and Richards (1975).

4 Field aspects and petrography of the Val Biandino Intrusive Suite

The intrusive rocks of the VBQD and VSBG, together with their hosting Variscan metamorphic basement, crop out in a tectonic window (Froitzheim et al., 2008) within the Permian volcanic and sedimentary succession (Fig. 2). The basement-cover contact is tectonic along the Grassi Shear Zone, or stratigraphic in the hangingwall of the same structure (Fig. 2). To the north and west of Cima d'Agrella (Fig. 2) the Verrucano Lombardo directly overlies in non-conformity the metamorphic basement and the Early Permian intrusive rocks of the VSBG, these ones showing evidence of exposure (paleosoils) at the surface before the deposition of the Verrucano Lombardo (Sciunnach, 2001a). Elsewhere the contact between the basement and the cover rocks is almost invariably marked by a ductile shear zone (the Grassi Shear Zone, GSZ, in Fig. 2), locally overprinted by cataclastic deformation, that has been interpreted as a detachment fault (Froitzheim et al., 2008; Pohl et al., 2018).

Both the VBQD and the VSBG intruded the Southalpine basement which reached amphibolite facies metamorphic conditions during the Variscan orogenic cycle (Milano et al., 1988; Diella et al., 1992). The basement mainly consists of two-mica paragneiss (Morbegno Gneiss; Cornelius, 1916) with minor micaschists, quartzites and amphibolites. The equilibrium mineralogical association at peak conditions consists of Qz + Pl + Bt + Chl + Ms + Gar + Ky + St (Froitzheim et al., 2008; mineral abbreviation here and in all the text after Whitney & Evans, 2010). Retrogression at lower greenschist facies conditions was completed during the Variscan orogenic cycle (Spalla et al., 1999; Zanoni and Spalla, 2018).

Along the Grassi Shear Zone (GSZ, Fig. 2) the paragneiss displays a mylonitic fabric with a well-developed stretching lineation. Biotite is replaced by chlorite that, together with muscovite, marks the mylonitic foliation. The stretching lineation, W of Rif. Grassi (Fig. 2), is highlighted by the occurrence of quartz rods, up to 20–25 cm in length (Fig. 3a). Finite strain associated with the GSZ rapidly decreases away from the contact, as highlighted by the occurrence of small-scale isoclinal folds that have been completely transposed within the shear zone. In the GSZ segment close to the Rif. Grassi, the mylonites are overprinted by brittle deformation associated with the development of cataclastic bands displaying a S-verging reverse motion, that affect both the basement and the overlaying Monte Cabianca Volcanite Small scale, asymmetric SE-verging folds interpreted as coeval with this brittle deformation phase, also occur. The vergence of these folds and the fact that they display brittle slip along their long limbs with kinematic indicators pointing to a S-vergent hanging wall motion (Fig. 3b), are consistent with the kinematics of the Late Cretaceous-Paleocene Orobic Thrust (Fig. 2; Zanchetta et al., 2011; Zanchetta et al., 2015).

4.1 The Val Biandino Quartz-Diorite (VBQD)

The VBQD consists of several stocks and minor lenses of mafic to felsic magmatic rocks that crop out in area comprised between Valtorta and Cortabbio (Fig. 2). Quartz-diorite, diorite and gabbro-diorite form the main bodies of the VBQD (A, B, C and D in Fig. 2; following De Capitani et al., 1988), with granodiorite chiefly occurring within bodies A and D.

Field surveys revealed that felsic types such as granite, two-mica leucogranite and aplitic dikes are confined at the rims of the main bodies, postdating their emplacement (Fig. 4a).

Diorite and quartz-diorite are the most abundant magmatic types. They are usually medium-grained to fine-grained with an isotropic texture (Fig. 4b). A poorly-developed magmatic foliation has been observed at the rims of bodies A and D, marked by the shape preferred orientation of biotite crystals. The magmatic phase assemblage consists of Pl + Bt + Amp + Qz + Kfs + Ap + opaque minerals (Fig. 5 and Table 1). The occurrence of orthopyroxene in these rocks is reported by De Capitani et al. (1988), but was not observed in the samples from this study, even if cummingtonite has been recognized in several samples, and may represents the alteration product after hydration of orthopyroxene.

Plagioclase is almost invariably zoned, mainly occurring as the interstitial phase between biotite and amphibole. Biotite occurs as highly pleochroic crystals with a reddish brown colour. Amphibole occurs in prismatic crystals reaching a few millimetres in length and are often partially replaced by biotite (Fig. 5a).

Gabbro-diorite form small stocks to the south of body B (Fig. 2) and at the southern margin of stock C. The magmatic assemblage is similar to that described for diorite and quartz-diorite except for the lack of biotite and K-feldspar. The occurrence of gabbro has been reported by Pasquarè (1967) within stock C (Fig. 2), but, based on our observations, only gabbro-diorite and diorite crop out there.

Granite and granodiorite are less abundant than mafic-intermediate rocks, with granodiorite that mainly occurs

Fig. 3 **a** Mylonites with quartz rods related to the Grassi Shear Zone (GSZ, Fig. 2) in the hosting basement of the VBQD; **b** Fault planes with a top-to-SE reverse motion developed in the paragneiss of the Variscan basement close to Rif. Grassi (Fig. 2); **c** Brittle planes overprint the quartz fabric related to subgrain rotation recrystallization in the mylonites of the Grasi Shear Zone

in the northern area of body A (Fig. 2) and, to a minor extent, as small lenses within body D, despite the fact that this magmatic body is historically known as the "Cortabbio Granodiorite" no clear crosscutting relationships have been observed between the granodiorite and mafic types, but the occurrence of dioritic and tonalitic enclaves within a granodiorite body SW of Rif. Grassi (Fig. 2) suggests that more differentiated rocks are younger or at least coeval with respect to diorite and quartz-diorite. The magmatic phase assemblage of studied granodiorite samples is made of Qz + Kfs + Bt + Pl ± Amp ± Ms + Ap + Zrn + opaque minerals. Granodiorite of the VBQD show the same mineralogical and fabric features across the whole complex. They are medium grained with an isotropic texture. An oriented fabric is seldom observed within sills at the rims of body D, intruded parallel to the main foliation in metamorphic host rocks. In these cases, the shape preferred orientation of biotite marks a poorly defined magmatic foliation parallel to sills rims.

The occurrence of two plagioclase generations is a common feature. The first one shows large crystals (up to 10 mm) typically with saussurite growing on Ca-rich cores and sericite replacing Ca-poor rims. The second generation, usually almost completely preserved, is made up of smaller interstitial plagioclase frequently displaying an albite twinning (Fig. 5b). Chlorite and sericite are present as alteration products on biotite and K-feldspar, respectively. Myrmekitic rims frequently occur along boundaries between K-feldspar and plagioclase or K-feldspar and quartz. Amphibole in the granodioritic types are partially substituted by biotite.

The VBQD comprises also two-mica leucogranite and aplitic dikes. Two-mica granitic lenses and dikes are mainly concentrated along the rims of bodies A and B. They occur as small lenses and dikes up to several

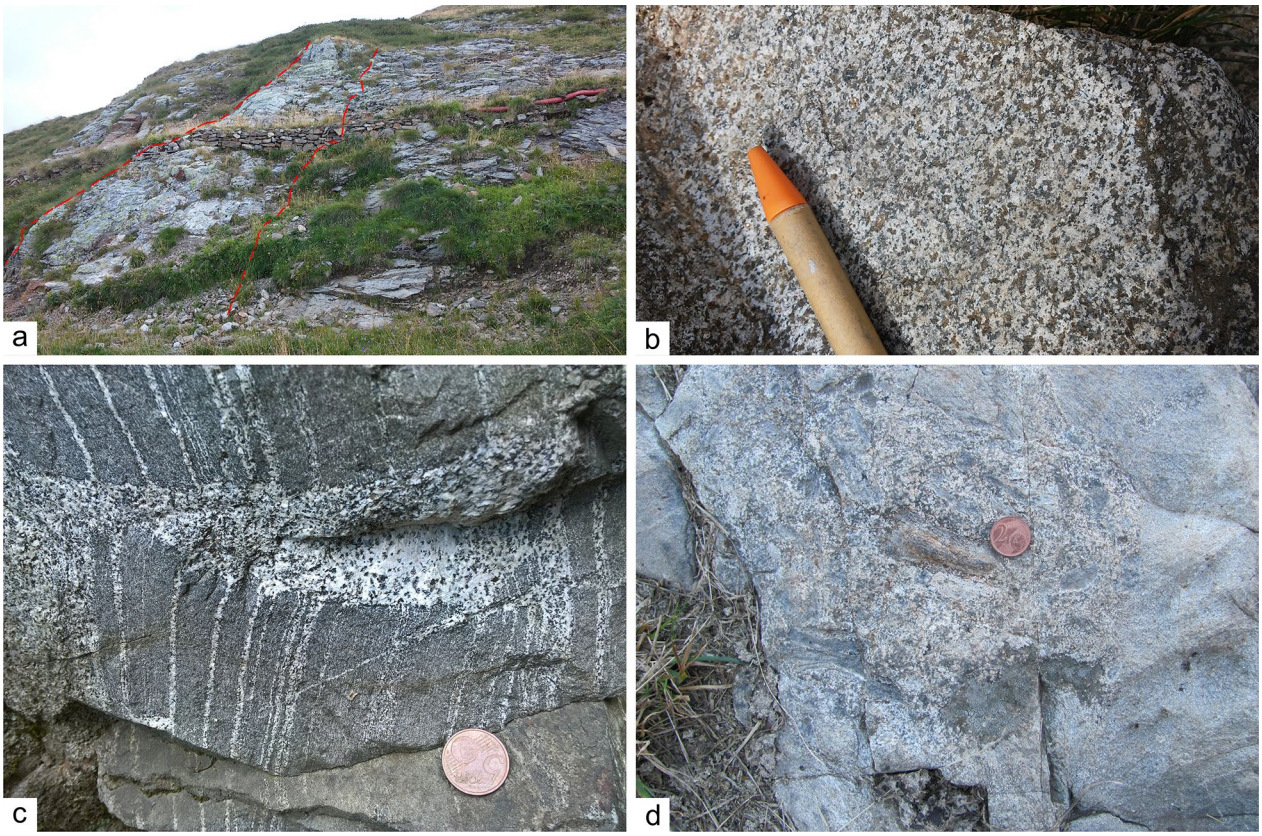

Fig. 4 Field aspect of the VBQD intrusive rocks. **a** Leucocratic granitic dike intruding the Variscan basement just S of Rif. Grassi (Fig. 2); **b** The quartz-diorite of stock A (Fig. 2) as observable in the field; **c** Quartz-diorite of stock D (Fig. 2) intruding the basement paragneiss with apophyses of the main body that crosscut the regional foliation and sills of a few mm in thickness that expand along the foliation planes; **d** Basement xenoliths in the VBQD granodiorite (sample VBZ32, Fig. 2) that is in turn included in a granite dike

meters in thickness (Fig. 4a). Granite are usually fine-grained and equigranular, with a typical magmatic assemblage made of Qz + Kfs + Pl + Ms + Bt ± Crd ± Ap ± Zrn ± Aln ± Ttn + opaque minerals. Epidote, chlorite and calcite occur as secondary phases. The presence of cordierite (Fig. 5c) suggests a peraluminous character for the granite, whose significance will be discussed in detail in Sect. 7.2.3. If the crosscutting relationships between dioritic and granodioritic bodies are unclear, the intrusion of the two-mica leucogranite clearly postdates the main mafic and intermediate magmatic bodies. This is clear at the NE margin of stock A, where crosscutting relationships between intermediate rocks and late-stage granitic and leucogranitic dikes can be observed. Here dioritic to tonalitic enclaves with more or less equidimensional shape and angular edges, are hosted in a granitic mass, containing also basement xenoliths made of partially digested paragneiss, showing evident signs of partial melting (Fig. 4d). Other inclusions are made of polycrystalline quartz nodules and minor granodiorite with abundant biotite.

4.2 The Val di San Biagio Granite (VSBG)

The VSBG crops out in the central part of Valsassina, north of the VBQD (Fig. 2). The VSBG consists of a coarse-grained pink-coloured granite (Fig. 6a), with a typical porphyric texture. The mineralogy is Qz + Kfs + Pl + Bt ± Ms + Zrn + Ap + opaque minerals. Degassing cavities, filled with quartz, calcite and zeolites commonly occur close to the contact with the hosting basement rocks. Mafic and dioritic enclaves, together with basement xenoliths, are quite common in the southernmost body, close to the Sassi Rossi Normal Fault (SRNF in Figs. 2, 6b), but only rarely observed elsewhere. The Sassi Rossi Normal Fault is characterized by a several decimetres thick cataclasites, mainly developed at the expense of rocks in the footwall of the fault plane. Locally, the cataclasites are impregnated by dark brown to black tourmalinite (Fig. 7), a feature already reported from other Permian faults close to magmatic rocks (e.g. Zhang et al., 1994; De Capitani et al., 1999; Zanchi et al., 2019; Locchi et al., 2022, Zanchetta et al., 2022). The SRNF terms abruptly both toward NE and S (Fig. 2) where the

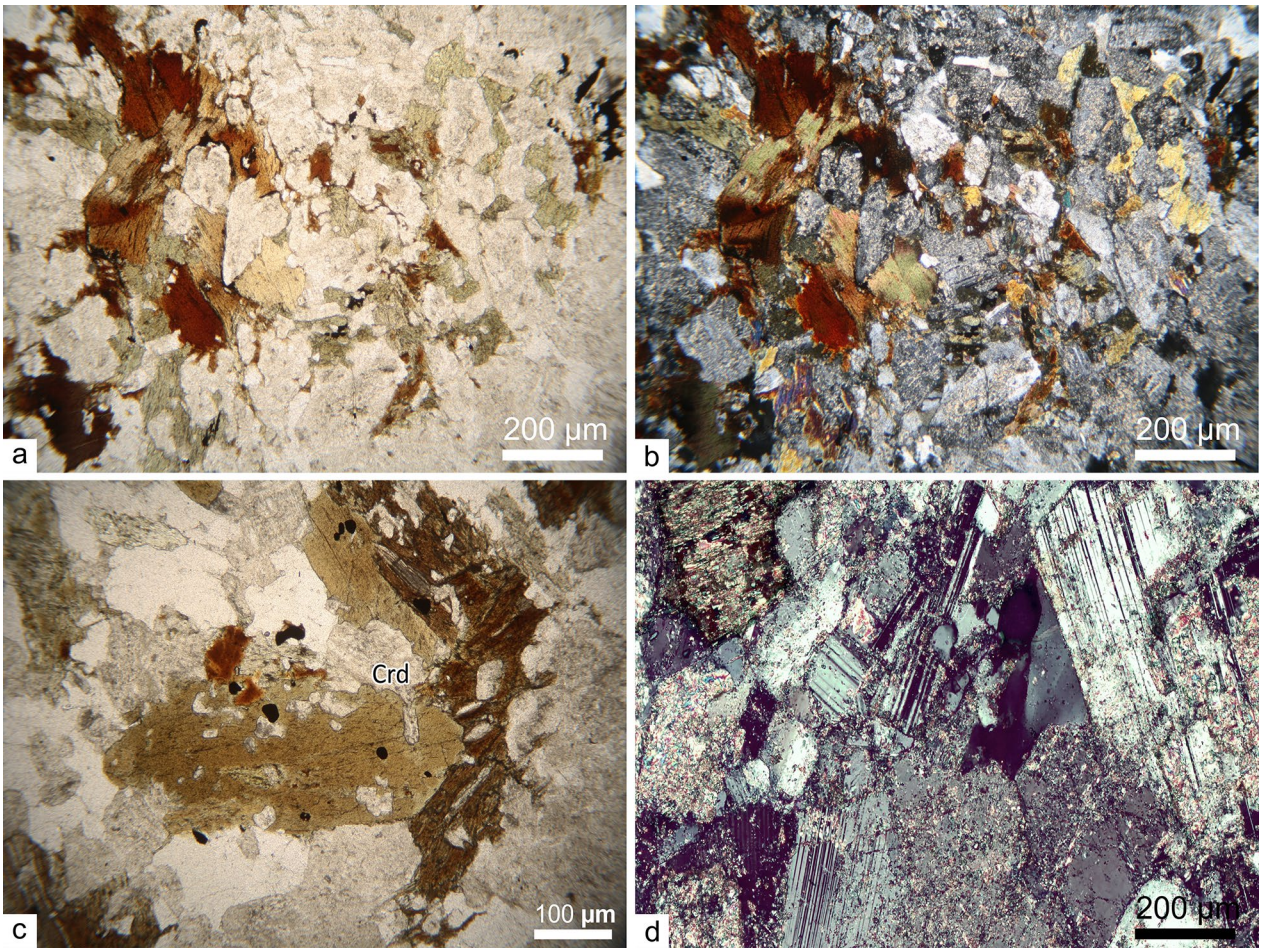

Fig. 5 Quartz-diorites of the VBQD **a** at parallel polars. **b** two generation of plagioclase with large crystals (Pl 2) having a saussuritized core and Ab-rich second generation forming smaller interstitial crystals with polysynthetic twin. **c** Cordierite crystals within the granites of the VBQD; **d** same as (**c**) at crossed polars

Verrucano Lombardo rests in non-conformity directly on the fault plane. These field relationships suggest that the SRNF was active in a time interval comprised between the intrusion of the VSBG and the deposition of the Lopingian Verrucano Lombardo (Sciunnach, 2001b).

4.3 Contact metamorphism associated to the Val Biandino Quartz-Diorite

Thermal metamorphism associated with the emplacement of the Val Biandino intrusives affected the hosting paragneiss up to 150–200 m away from the magmatic bodies. The first observable effect is the crystallization of a new generation of muscovite and biotite, growing statically on the Variscan foliation. Biotite along the regional foliation appears strongly decoloured, whereas the second generation occurs both as fresh single flakes and as pluri-millimetric aggregates (Fig. 8a), made by tabular lamellae of red-brownish Ti–rich biotite. A second generation of muscovite has been also observed in some samples.

Small sillimanite crystals with a prismatic habit (Fig. 8c and d) have been recognized in samples collected less than 80 m from the contact between the paragneiss and the diorite of body B (Fig. 2). The occurrence of andalusite and cordierite in biotite gneiss within the contact aureole was reported by Pasquarè (1967) in the host rocks of body C (Fig. 2), but neither minerals have never been observed in our samples. The recognition of cordierite could be hampered by the fact that it is easily replaced by pinite (chlorite + muscovite, Fig. 8b), especially if late-stage hydrothermal fluids circulated during the final stage of pluton emplacement, as suggested by the observed occurrence of tourmaline-bearing quartz veins close to the intrusive contact of bodies A and D. Newly formed, thin K-feldspar rims around plagioclases occur in paragneiss as far as ca. 100 m from the intrusive contact.

Table 1 Samples location and petrography

	Gauss-Boaga		WGS84			
Sample	**Long.**	**Lat.**	**Long.**	**Lat.**	**Rock type**	**Mineralogy**
VBQD						
VBZ-1	1,535,862	5,092,881	9.462673	45.988375	Leucogranite (B)	Qz, Kfs, Plg, Bt, Ms, Crd, Zrn, Ilm, Ap (*Chl, Ab, Fe-oxides*)
VBZ-3	1,535,902	5,093,053	9.463203	45.989921	Leucogranite (B)	Qz, Kfs, Plg, Bt, Ms, Zrn, Ilm, Ap (*Chl, Ab*)
VBZ-11	1,537,934	5,094,773	9.489575	46.005292	Quartz-Diorite (A)	Plg, Bt, Amp, Qz, Kfs, Ap, Ilm, Zrn (*Chl, Ab, Fe-oxides*)
VBZ-16	1,537,693	5,095,465	9.486517	46.011533	Quartz-Diorite (A)	Plg, Bt, Amp, Qz, Kfs, Ap, Ilm, Zrn (*Chl, Fe-oxides*)
VBZ-32	1,537,282	5,095,484	9.481210	46.011726	Granodiorite (A)	Qz, Kfs, Plg, Bt, Amp, Ap, Zrn (*Chl, Fe-oxides*)
VBZ-35	1,536,241	5,092,042	9.467503	45.980805	Leucogranite (B)	Qz, Kfs, Plg, Ms, Bt, Crd, Zrn, Ilm, Ap (*Chl, Ab*)
VBZ-36B	1,536,237	5,092,019	9.467450	45.980598	Granodiorite (B)	Qz, Kfs, Plg, Bt, Amp, Ap, Zrn (*Chl, Fe-oxides*)
VBZ-37	1,536,209	5,091,965	9.467084	45.980113	Gabbro-diorite (B)	Plg, Amp, Bt, Ap, Ilm, Ep (?) (*Chl, Ab, Fe-oxides*)
VBZ-40	1,531,436	5,093,420	9.405564	45.993443	Quartz-Diorite (D)	Plg, Bt, Amp, Qz, Kfs, Ap, Ilm, Zrn (*Chl, Fe-oxides*)
VSBG						
VBZ-42	1,530,590	5,094,073	9.395233	46.044096	Porphyric granite	Kfs, Qz, Plg, Ms, Ap, Zrn (*Ab, Fe-oxides*)
VBZ-43	1,530,012	5,095,570	9.387311	46.012857	Porphyric granite	Kfs, Qz, Plg, Ms, Bt, Ap, Zrn (*Ab, Fe-oxides*)

A,B,C,D refer to the intrusive bodies of Fig. 2

Coordinates are both in the Gauss-Boaga reference system (Monte_Mario_1_Italy, expressed in meters) and in the WGS84 reference system

Secondary minerals in italic. All abbreviation from Whitney and Evans (2010)

The foliated fabric of hosting paragneiss is completely obliterated within 10–15 m from the intrusive contact, with paragneiss that are replaced by massive dark-gray coloured hornfels, sometimes with bluish shade. Small (up to 150 μm of diameter) subeuhedral corundum crystals (Fig. 8c and d) have been recognized in one sample. The occurrence of corundum formed in response to the thermal metamorphism in the contact aureole of a Southalpine Permian intrusion has been also reported by Whylidal et al. (2012) for the contact aureole of the Brixen granodiorite. The occurrence of corundum suggests temperature above 680 °C reached in the close proximity of the margins of the intrusive bodies (Montel et al., 1986).

5 Geochemistry

A total of 11 samples where crushed and processed for bulk rock geochemical analysis. The analyses were performed on samples collected in different parts of the intrusive complex and selected to be representative of the lithological variety, from gabbro-diorite to granite (Table 2).

The SiO_2 content ranges from 52 wt% to 75 wt% and it is negatively correlated with the FeO and MgO contents (Fig. 9) that range 7–10 wt% and 5–10 wt%, respectively. Alkalis wt% ($Na_2O + K_2O$) varies from ca. 3 wt% in low-SiO_2 rocks, up to 7 wt% in granites of the VBQD (Fig. 9, Table 2) and more than 8 wt% in the VSBG granites (Table 2). K_2O is commonly higher than Na_2O, with the only exceptions of granodiorites of lenses A-D and the diorite of lens D (Table 2).

The TAS classification diagram and the K_2O-SiO_2 variation diagram indicate a high-K calc-alkaline affinity (Fig. 9a and b) for the rocks of the Val Biandino Intrusive Suite, as already pointed out by De Capitani & Liborio (1988) and Thöni et al. (1992). Our data and data available in the literature clearly show that the SiO_2 content of the VBQD and VSBG display some gaps, without a continuous trend from mafic to acidic types. Clusters occur around 52 wt%, 60 wt%, 67 wt% and 75 wt% (Fig. 9a and b). The implications of this pattern in terms of magma genesis will be discussed later. The Mg number is negatively correlated with the SiO_2 abundance, with some samples displaying very high values (sample VBZ-16, diorite, Table 2).

The VBQD and VSBG calc-alkaline affinity is also evident from trace elements, with LILE enrichment (100 to 1000 times PM, Primitive Mantle, values, Fig. 9c, d, e) with respect to HFSE, and LREE enrichment with respect to HREE (Fig. 9f, g, h). The PM-normalized negative anomalies of Nb, Ta and Ti are coherent with a volcanic arc magmatism (Gill, 1981), with values between 1 and 10 for Ti, 5 -50 for Nb and 9–50 for Ta (Table 2). However, the negative spikes of Nb, Ta and Ti are not coupled with positive spikes of Pb, Sr and Rb, as commonly recognized in volcanic arc magmatism (Gill, 1981). Rb and Th are enriched in the PM-normalized diagram (Fig. 9c, d, e) with respect to Ba, as already observed in calc-alkaline magmatism developed in extensional settings (Broutin et al., 1994).

LREE are significantly fractionated, mainly in leucogranites (Fig. 9h), with La/Sm_n up to ca. 5 (Table 2).

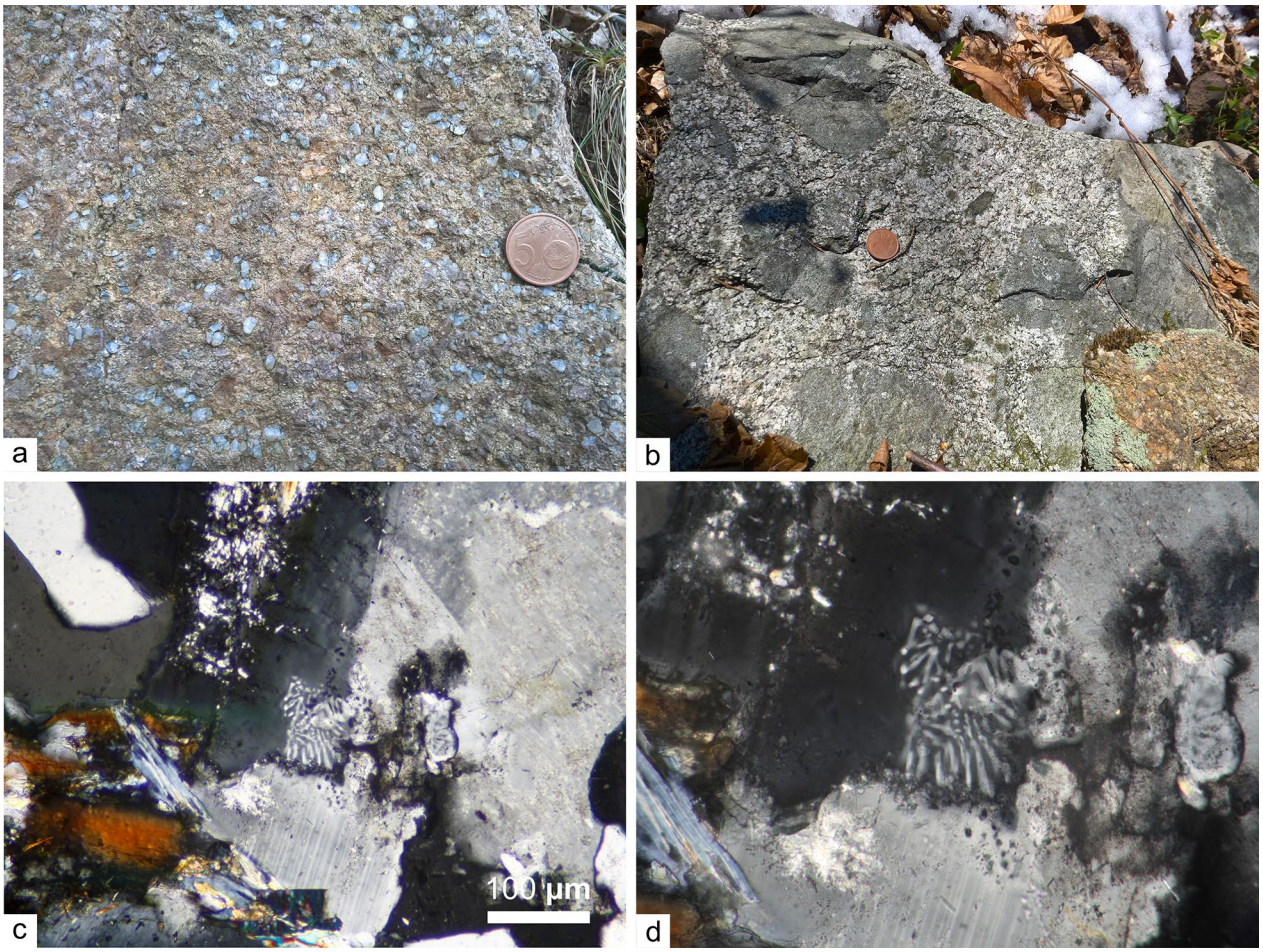

Fig. 6 **a** The typical porphyric texture of the VSBG granite as it appears in outcrops; b) The VSBG intruding Variscan basement NW of the SRNF (Fig. 2); **c** Myrmekites developed at the contacts between K-feldspar and plagioclase crystals; **d** detail of figure **c**

HREE fractionation is instead weak, with some samples that show a poorly outlined "spoon-like" pattern (Fig. 9f, g, h).

6 Geochronology

The intrusion age of the several bodies composing the Val Biandino Intrusive Suite has been dated by several authors from the'90 until recently. More recent results point to an intrusion age of 289.1 ± 4.5 Ma and 286.8 ± 4.9 Ma for the VBQD and the VSBG, respectively (U–Pb on zircon, Pohl et al., 2018). As the uncertainties associated with the available ages are quite large, we tried to obtain more intrusion ages for both the VBQD and the VSBG in area not sampled by previous works. Two samples, one granite from the VBQD (VBZ3) and one porphyric granite from the VSBG (VBZ43) have been selected.

The zircon grains of the VBQD sample (VBZ3) typically range in dimension from 50 up to 200 µm, with the largest ones displaying an elongated prismatic habit, whereas smaller crystals have usually sub-equant prismatic habit. Elongated crystals are richer in inclusions, mainly apatite and rutile, that occur less frequently in small zircons. The width-to-length ratios of larger crystals is 1:3 to 1:4, whereas smaller ones are typically 1:1.5 to 1:2.5. Cathodoluminescence imaging (Fig. 10) revealed an oscillatory zoning of magmatic origin (Corfu et al., 2003) for most of the crystals, with a few of them showing inherited cores and signs of resorption phenomena during the growth. The U content ranges from 208 to 1890 ppm, with the higher values recorded in the inner parts of the elongated crystals. The Th contents ranges from 88 to 990 ppm and it is generally positively correlated with the U content. The Th/U ratios are below 1 and above 0.1 for most of the analytical spots (all data are reported in Table 3). Single $^{206}Pb/^{238}U$ dates between 271.3 and 302.6 Ma (Table 3) have been measured in zircon grains of the VBZ3 granite, with 14/16 analytical

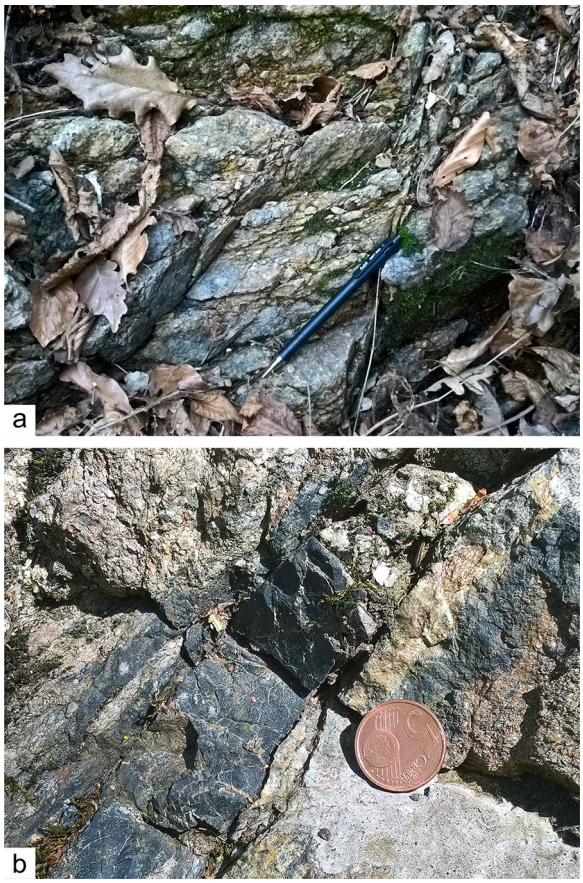

Fig. 7 **a** Foliated cataclasites along the Sassi Rossi Normal Fault (SRNF, Fig. 2); **b** Tourmalinite vein of ca. 2 cm thickness injected along the SRNF fault plane.

spots that provided dates < 290 Ma. The calculated concordia date, disregarding dates with more that 5% of discordance, is 285.2 ± 1.9 Ma (Fig. 10a).

Zircon crystals from the VBZ43 sample appear colourless or with a pale pink shade, mainly inclusion-free, with the exception of rare micrometric apatites. Most zircon grains display a subequant prismatic habit with a width-to-length ratio of 1:2–1:2.5 ranging in dimension from 150 to 200 µm. Rare crystals with an elongated prismatic habit reach 300–350 µm, with a width-to-length ratio of about 1:5. In these crystal inclusions are more frequent, mainly consisting of apatite and rutile. Cathodoluminescence imaging revealed a typical oscillatory zoning of magmatic origin (Corfu et al., 2003) for most of the zircon, grains with more complex zoning displayed by a few subequant grains larger than 200 µm (Fig. 10). The U contents of measured spots range from 197 to 2028 ppm (Table 3), with higher values related to the outer rim of elongated crystals. Sevently percent of the measured spots have U-contents below 600 ppm. Th ranges 97–540 ppm, and it is positively correlated with U, except for the spots with U > 1500 ppm. The Th/U ratios are always below 1 and above 0.1. Zircons from the VSBG porphyric granite (sample VBZ43) gave single $^{206}Pb/^{238}U$ dates between 273.1 and 290.2 Ma (Table 3), with 16/20 analytical spot yielding dates younger than 285 Ma. The calculated concordia date is 283.2 ± 1.9 Ma (Fig. 10b).

7 Discussions

7.1 The Val Biandino Intrusive Suite and the Early Permian magmatism in the Southalpine Domain

In the Val Biandino Intrusive Suite, the main rock varieties are represented by metaluminous to peraluminous high-K calc-alkaline quartz-diorite, granodiorite and granite. Metaluminous high-K calc-alkaline gabbro-dioritic stocks also occur in the eastern area of the complex (Fig. 2). S-type cordierite leucogranite and peraluminous high-K calc-alkaline muscovite leucogranitegranite form small stocks and dikes intruding the mafic to intermediate rocks. North of the VBQD, the emplacement of the 283.2 ± 1.9 Ma (Fig. 10b) VSBG granite possibly marks the end of the intrusive magmatic activity in the area as the occurrence of other magmatic bodies has never been reported. This is hypothesis is also supported by the occurrence of Middle Permian inversion tectonics and the almost complete lacking of sediments and volcanic products of the same age in the central Southern Alps (Gaetani et al., 1986) The onset of subaerial volcanic activity in the Orobic Basin (central Southern Alps, Fig. 1) is constrained at ca. 280 Ma (Gretter et al., 2013; Berra et al., 2015) and likely ended at 270 ± 2 Ma (ignimbritic flows at the top of the Monte Cabianca Volcanite, U–Pb zircon age, Berra et al., 2015). In the study area the "Ponteranica conglomerates", bearing clast of volcanic rocks, of the Pizzo del Diavolo Formation and the Monte Cabianca Volcanite rest below the Verrucano Lombardo (Fig. 2), but their field relationships with the VSBG are not observable.

The Permian magmatism occurs extensively in the western Southern Alps (WSA in Fig. 1). Mafic (gabbro) to intermediate (norite and diorite) rocks mainly occur in the Ivrea Verbano Zone (Lower and Upper Mafic Complex; e.g., Rivalenti 1975; Sinigoi et al., 1991; Peressini et al., 2007; Sinigoi et al., 2011), whereas eastwards granitic and hypabyssal granitic bodies ("Graniti dei Laghi" and Valganna granophyric granite) intrude the basement of the Serie dei Laghi (e.g., Bakos et al., 1990; Pinarelli & Boriani, 2007) (Fig. 1).

Comparing the mafic to intermediate rocks of the Ivrea Verbano Mafic Complex, at any given SiO_2 content they are less enriched in K_2O (Fig. 11) than the Val Biandino ones, though they have similar REE patterns (Fig. 12). Minor anatectic granitic bodies, showing similar geochemical features to the leucogranite of

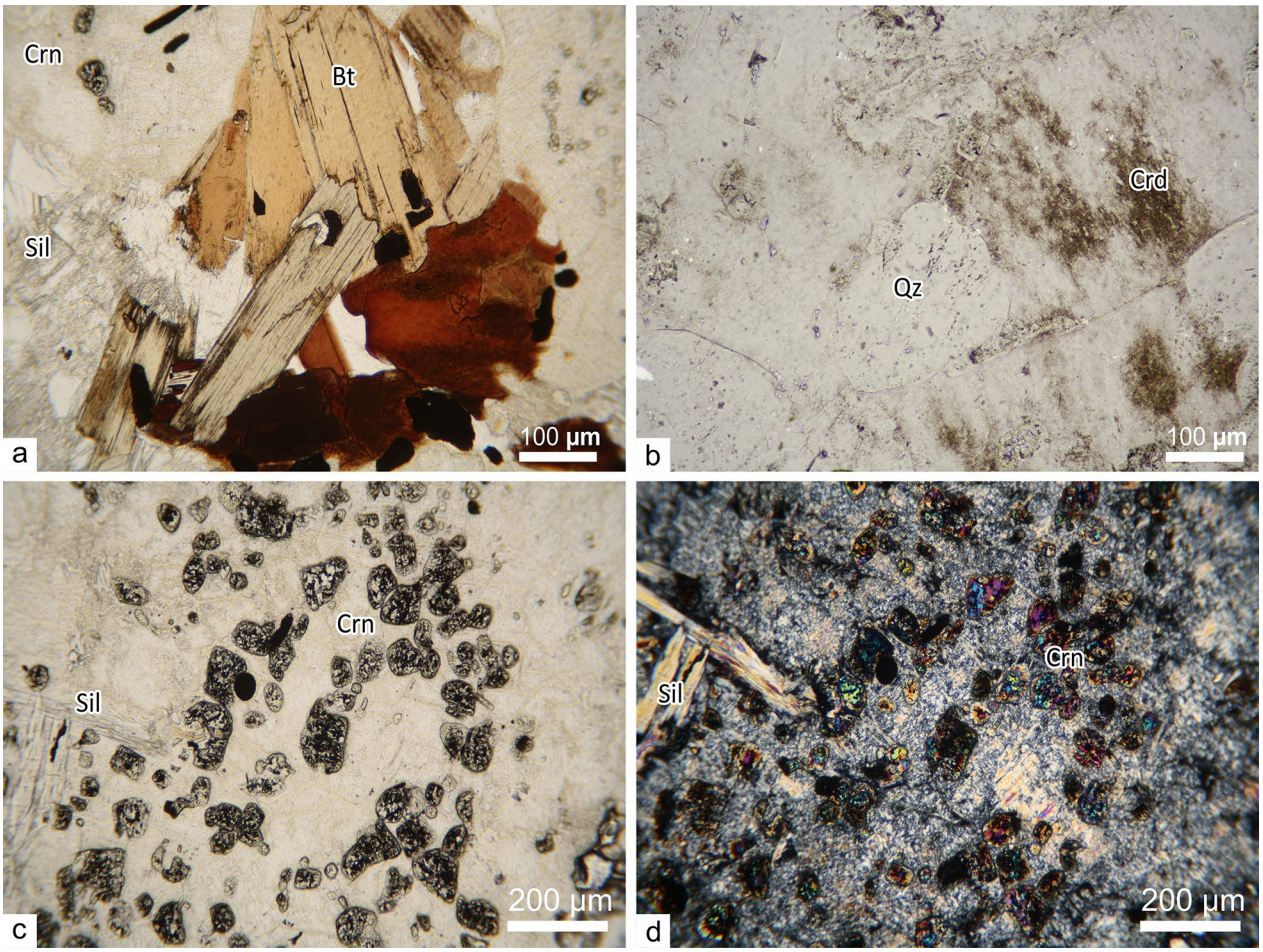

Fig. 8 **a** Static overgrowth of biotite crystals in the thermal aureole of the VBQD on pre-existing biotite in the host paragneisses, close to the contact with stock A (Fig. 2). **b** Pinite + quartz aggregates after cordierite in the basement paragneisses (stock B, Fig. 2). **c** Statically growth of corundum (Crn) and sillimanite (Sil) within the contact aureole. **d** Figure (**c**) at crossed polars. The size of the corundum crystals allow to rule out a contamination during thin sections preparation and polishing

the Val Biandino Intrusive Suite, also occur (Fig. 11a, b). U–Pb zircon analyses have provided emplacement ages of ca. 285 Ma (Sinigoi et al., 2011) and 293 ± 6 Ma (Vavra et al., 1999) Ma for amphibole gabbros of the Lower Mafic Complex, of 287 ± 3 Ma for an interlayered norite (Quick et al., 2003; Peressini et al., 2007), of 286–289 Ma (Peressini et al., 2007) for a gabbro of the Upper Mafic Complex, and of 288 ± 3 (Quick et al., 2003) and 285 ± 7 Ma (Pin, 1986) for biotite-rich monzogabbros historically referred to as "diorites" in the literature (Rivalenti, 1975) (Fig. 13). To the east of the Ivrea Vebano Zone, large calc-alkaline granitic subvolcanic bodies, represented by the Graniti dei Laghi (e.g., Pinarelli & Boriani, 2007) and the Valganna granophyric granite (e.g., Bakos et al., 1990), are enriched in K_2O, LREE and HREE contents and show flat REE patterns with a more pronounced Eu anomaly than the Val Biandino leucogranite (Fig. 12). The "Graniti dei Laghi" emplaced at 282 ± 1.5 Ma (Montorfano, U–Pb zircon ages, Schaltegger & Brack, 2007), 272–279 Ma (Baveno, Rb–Sr WR-Bt, Pinarelli et al., 2002), 289 ± 3.4 Ma (Roccapietra, U–Pb zircon age, Quick et al., 2009), 273–280 (Valle Mosso, U–Pb zircon ages, Quick et al., 2009) and 281–298 Ma (Valle Mosso, U–Pb zircon age, Klötzli et al., 2014). An emplacement age of 281.3 ± 0.5 Ma (U–Pb zircon age, Schaltegger & Brack, 2007) is instead reported for the Valganna granophyric granite (Fig. 13).

A swarm of mafic to acidic dikes and small hornblende-diorite stocks (Appinites, Pinarelli & Boriani, 2007) emplaced between 312–278 Ma (U–Pb zircon age, Klötzli et al., 2014) near the contact of the Serie dei Laghi and the Ivrea Verbano Zone (Fig. 13). The bimodal volcanic activity in the western Southern Alps persisted from 290 to 282 Ma (U–Pb zircon age, Quick et al., 2009) in the Sesia Valley and from 298 to 288 Ma (U–Pb zircon ages, Schaltegger & Brack, 2007) in the Valganna district.

Table 2 Whole rock major (oxide %) and trace element (ppm) abundances in the analysed samples of the Val Biandino Intrusive Complex

	VBQD—Val Biandino Quartz-Diorite									VBSG—Val San Biagio Granite	
Rock type	**Gabbro-diorite B**	**Diorite A**	**Diorite A**	**Diorite D**	**Granodiorite A**	**Granodiorite B**	**Granite B**	**Granite B**	**Granite B**	**Granite SBG**	**Granite SBG**
Sample	**VBZ-37**	**VBZ-11**	**VBZ-16**	**VBZ-40**	**VBZ-32**	**VBZ-36B**	**VBZ-1**	**VBZ-3**	**VBZ-35**	**VBZ-42**	**VBZ-43**
SiO_2	52.14	53.77	51.86	58.10	58.97	67.81	73.33	73.06	74.96	68.51	73.49
TiO_2	0.80	0.95	0.55	0.98	0.87	0.50	0.19	0.23	0.21	0.34	0.23
Al_2O_3	16.97	18.10	11.21	17.48	18.64	16.03	14.70	14.87	13.02	15.61	14.08
FeO*	7.40	7.14	9.18	6.30	5.94	3.23	1.34	1.49	1.41	2.77	1.76
MgO	7.29	5.32	16.40	3.65	2.60	1.37	0.47	0.47	0.44	0.46	0.35
CaO	7.07	5.42	4.29	5.62	4.64	1.87	1.38	1.90	0.65	1.68	0.09
Na_2O	2.08	2.31	1.16	2.94	3.36	3.72	3.02	3.20	2.29	3.66	2.41
K_2O	2.25	2.58	1.99	2.20	2.47	3.21	4.22	4.02	5.25	4.86	5.50
P_2O_5	0.07	0.13	0.05	0.21	0.26	0.15	0.06	0.05	0.22	0.07	0.04
MnO	0.15	0.16	0.18	0.13	0.10	0.07	0.03	0.03	0.03	0.05	0.07
Mg no	49.64	42.68	64.12	36.69	30.45	29.78	25.96	23.93	23.75	14.24	16.56
LOI	2.54	3.18	2.55	2.34	2.14	1.59	0.99	0.74	1.01	1.07	2.11
Sc	29	21	35	20	9	8	4	4	5	15	6
V	188	168	223	136	102	41	12	15	21	21	16
Cr	230	0	1000	60	20	bd	bd	bd	bd	bd	bd
Co	29	23	62	16	12	7	2	2	4	3	3
Ni	50	20	320	20	bd	bd	bd	bd	bd	bd	bd
Ga	16	19	11	20	22	17	17	18	12	23	17
Rb	92	108	73	77	104	83	185	161	126	107	168
Sr	242	242	122	400	366	343	150	229	211	149	45
Y	20	21	10	21	13	20	13	11	12	33	24
Zr	109	141	66	223	189	175	97	105	76	346	170
Nb	5	7	2	10	10	9	6	6	6	14	10
Ba	263	330	420	560	467	678	469	574	873	1701	499
Cs	5.2	7.7	7.1	3.6	5.8	1.6	6	4.7	3.8	3.3	10.1
La	14.4	19.5	8	26.6	26.4	30.6	34.9	35.3	12.3	83.3	32.8
Ce	30.4	41.2	16.6	54.2	51.7	62.1	66.2	67.9	23.7	163	66.3
Pr	4.02	5.04	2.02	6.37	5.61	6.87	7.01	7.36	2.66	17.6	7.21
Nd	17.3	21.2	8.7	25.1	20.7	25.7	25.7	26	10.1	65.6	26.6
Sm	3.7	4.6	1.9	5.3	3.4	4.9	4.9	4.8	2.1	11.7	5.5
Eu	1.18	1.32	0.55	1.57	1.6	1.11	0.83	0.99	1.28	2.26	0.76
Gd	3.7	4.3	2	4.5	2.7	4.2	3.5	3.4	1.9	8.9	4.6

Table 2 (continued)

	VBQD—Val Biandino Quartz-Diorite									VBSG—Val San Biagio Granite	
Rock type	**Gabbro-diorite B**	**Diorite A**	**Diorite A**	**Diorite D**	**Granodiorite A**	**Granodiorite B**	**Granite B**	**Granite B**	**Granite B**	**Granite SBG**	**Granite SBG**
Sample	**VBZ-37**	**VBZ-11**	**VBZ-16**	**VBZ-40**	**VBZ-32**	**VBZ-36B**	**VBZ-1**	**VBZ-3**	**VBZ-35**	**VBZ-42**	**VBZ-43**
Tb	0.6	0.7	0.3	0.7	0.4	0.7	0.5	0.5	0.4	1.3	0.8
Dy	3.6	4.1	1.9	4.1	2.3	3.7	2.4	2.3	2.2	7	4.6
Ho	0.7	0.8	0.4	0.8	0.5	0.7	0.4	0.4	0.4	1.3	0.9
Er	2.1	2.2	1.2	2.2	1.3	1.9	1.2	1	1.3	3.5	2.5
Tm	0.3	0.34	0.17	0.32	0.2	0.29	0.17	0.15	0.21	0.45	0.38
Yb	1.9	2.3	1.1	2.1	1.4	1.7	1.1	0.9	1.5	3	2.7
Lu	0.32	0.35	0.17	0.33	0.23	0.28	0.16	0.14	0.24	0.47	0.39
Hf	2.3	3.1	1.3	4.7	3.7	3.8	2.4	2.4	1.6	7.6	4.1
Pb	6	1	1	11	18	26	25	26	47	16	21
Th	3.6	7.8	2.1	6.5	7.1	10.9	15.6	14.5	3.6	14.5	19.7
U	1.3	1.6	0.5	1.6	1.8	3	3.1	2.8	1.4	1.6	4.9
Ta	0.3	0.5	0.2	0.7	0.7	1.2	0.8	0.6	1.2	0.7	1.2
ΣREE	84.22	107.95	45.01	134.19	118.44	144.75	148.97	151.14	60.29	369.38	156.04
ΣLREE	69.82	91.54	37.22	117.57	107.81	130.17	138.71	141.36	50.86	341.2	138.41
ΣHREE	3.38	3.95	1.83	4.17	2.47	3.92	3.34	3.26	1.66	8.43	4.21
Eu/Eu*	0.97	0.91	0.86	0.98	1.61	0.75	0.61	0.75	1.96	0.68	0.46
$(La/Yb)_n$	5.44	6.08	5.22	9.09	13.53	12.91	22.76	28.13	5.88	19.92	8.71
$(La/Sm)_n$	2.51	2.74	2.72	3.24	5.01	4.03	4.60	4.75	3.78	4.60	3.85
$(Gd/Yb)_n$	1.61	1.55	1.50	1.77	1.60	2.04	2.63	3.13	1.05	2.45	1.41

A,B,C,D refer to the intrusive bodies of Fig. 2

LOI Loss On Ignition, *FeO** total Fe expressed as $FeO^* = 0.8998 * Fe_2O_3$; Mg no. = MgO/(MgO + FeO*)x100 expressed in wt% with all Fe as FeO; *bd* below detection limit

n subscript—normalization to chondrite values (McDonough and Sun, 1995)

SLREE light rare earth element sum, *SHREE* heavy rare earth elements sum; $Eu/Eu^* = Eu_n / RADQ(Sm_n \times Gd_n)$

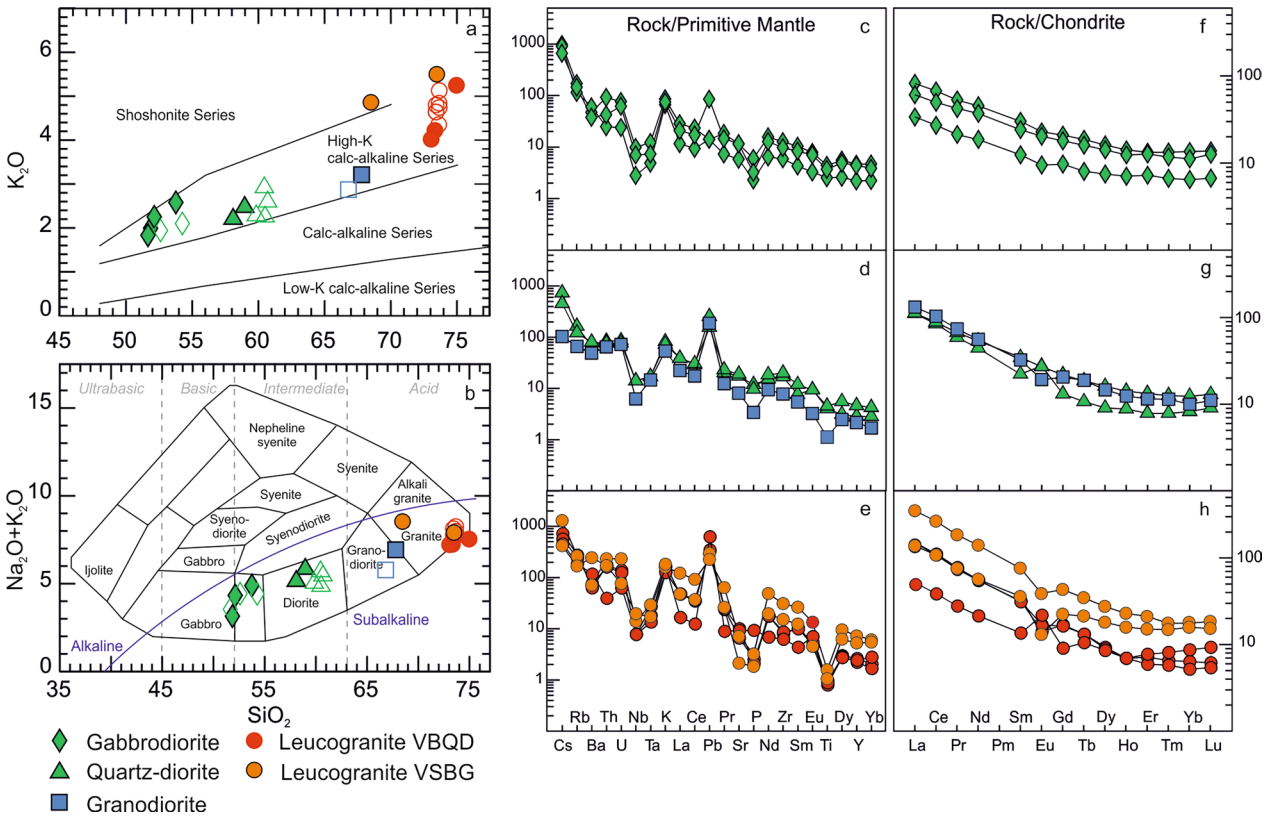

Fig. 9 **a** SiO_2 vs. K_2O wt% diagrams displaying the high-K calc-alkaline affinity of the VBQD and VSBG rocks; **b** alkali-silica classification diagram that shows the positive correlation between silica and alkali and also the gaps existing in the distribution of the SiO_2 content in the rocks of the VBQD

In the central Southern Alps, beside the Val Biandino intrusive Suite, small stocks of quartz-diorite, granodiorite to granite occur (De Capitani et al., 1994) (Val Navazze, Fig. 1). In this area, granodiorite and granite are enriched in K_2O, as well as in LREE and HREE contents, with a more pronounced negative Eu anomalies relative to our samples (Val Navazze, Fig. 12g).

In the Collio basin, east of the Orobic basin (Fig. 1) the volcanic activity started at 283 ± 2 Ma (U–Pb zircon age, Schaltegger & Brack, 2007) with ignimbrites and ended at about 280.5 ± 4 Ma (U–Pb zircon age, Schaltegger & Brack, 2007) with the emplacement of the Auccia volcanite. This latter age is in agreement with those determined for a dacitic flow and a rhyodacitic ignimbrite at the top of the successions in Val Daone (277.9 ± 2 Ma, U–Pb zircon age, Gretter et al., 2013) and in Val Rendena (279.2 ± 2 Ma, U–Pb zircon age, Gretter et al., 2013), respectively (Figs. 1, 13).

A large intermediate to acidic Permian magmatic activity took place also in the eastern Southern Alps (ESA in Fig. 1). The Permian intrusions are represented by the plutons of Cima d'Asta, Bressanone (Brixen), Ivigna (Ifinger), Monte Croce (Kreuzberg) and Monte Sabion (Fig. 1). These plutons mainly consist of high-K calc-alkaline granodiorites, monzogranites and S-type leucogranites, with minor tonalities (only at Cima d'Asta). Their emplacement ages have been constrained at 275.5 ± 3 Ma (U-Th allanite age, Barth et al., 1993) for a Cima d'Asta granodioritic sample; at 286.6 ± 2.9 and 293 ± 3 Ma (U–Pb zircon age, Bargossi et al. 2010; Morelli et al., 2012, respectively) for the Ivigna tonalities; at 285.4 and 284.3 ± 1.6 Ma (U–Pb zircon age, Marocchi et al., 2008) for the Monte Croce granodioritic and monzogranitic rocks, respectively. The emplacement age of the Mt. Sabion pluton (Figs. 1, 13) is constrained at 275 ± 9 Ma (Rb–Sr whole rock, Borsi et al., 1966). The Bressanone (Brixen) granodiorite and granite were emplaced at ca. 281 Ma (Rb–Sr whole rock, Del Moro & Visonà, 1982), with associated gabbroic bodies (the Lives, Luson and Chiusa gabbros) having the same age (281.8 ± 0.004, Boscaini et al., 2020). U–Pb zircon age of 277.9 ± 3.4 Ma have been obtained for the Canezza quartz-diorite-tonalite stock (Avanzini et al., 2010) (Fig. 13). Gabbros and diorites, showing medium- to high-K calc-alkaline affinity (Fig. 11), are reported only for the Bressanone (Brixen) and Cima d'Asta plutons. These rocks are locally

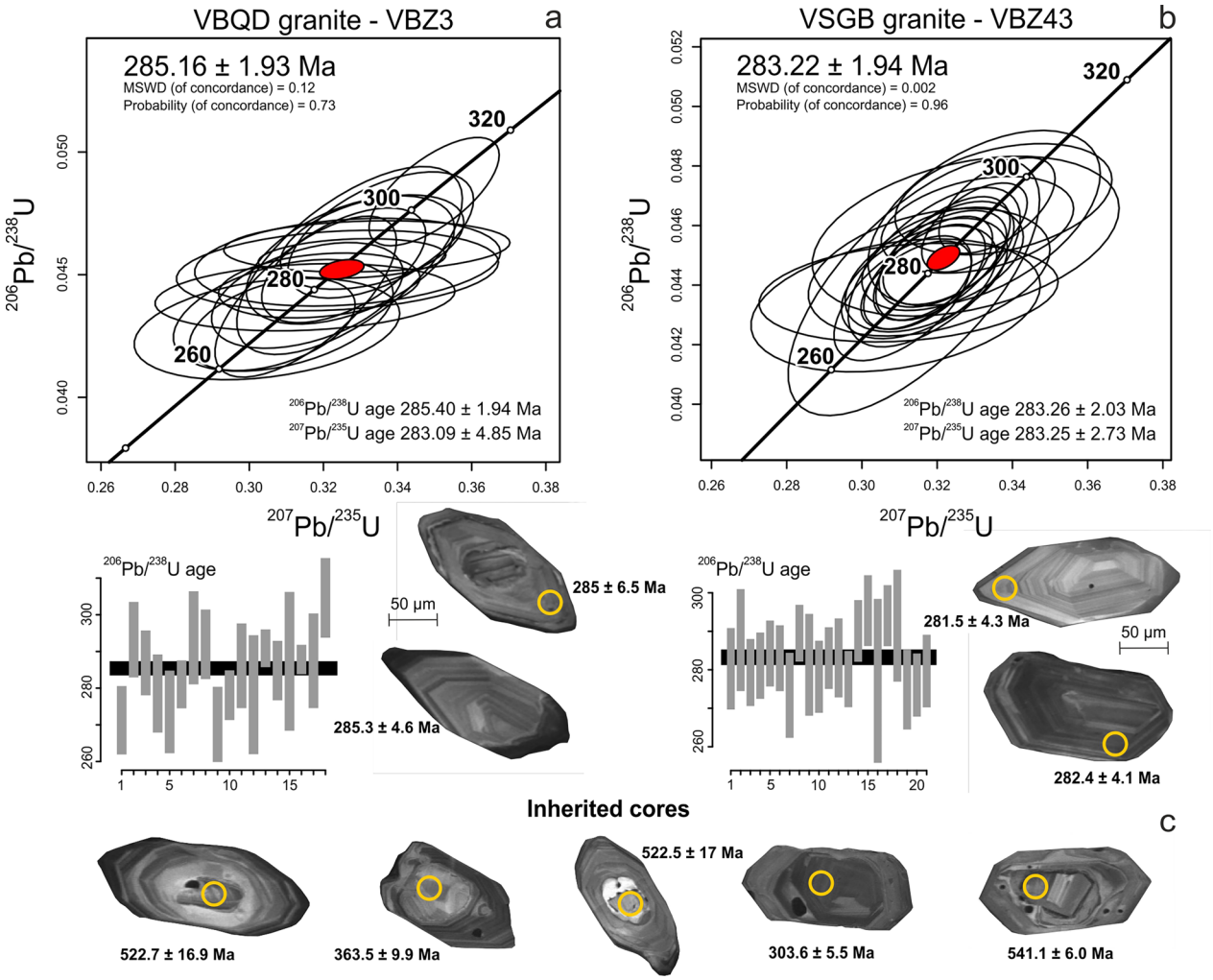

Fig. 10 SHRIMP U–Pb zircon ages of two granites from the VBQD (**a**) and VSBG (**b**) units. **c** Analytical spots on inherited cores within zircon grains. All spot ages are $^{206}Pb/^{238}U$ ages. Analytical results are reported in Table 3

associated with S-type cordierite granites. Del Moro & Visonà (1982) determined a Rb–Sr whole rock age of 286 ± 5 Ma for a cordierite granite within the Brixen pluton. At any given SiO_2 content, all these rocks show chondritic-normalized REE patterns similar to those of the Val Biandino Intrusive Suite (Fig. 12).

The volcanism, represented by the Athesian Volcanic district, started during the Early Permian at 290.7 ± 3 Ma (U–Pb zircon age, Visonà et al., 2007) and ended at 274.1 ± 1.6 Ma (U–Pb zircon age, Marocchi et al., 2008).

7.2 Petrogenesis

The Val Biandino Intrusive Suite, with its mafic components showing a magnesian-potassic affinity and its felsic ones displaying both peraluminous and S-type character, is similar to numerous high-K calc-alkaline mafic–felsic igneous associations worldwide (e.g., Bonin, 2004; Barbarin et al., 2005). Experimental arguments, field evidence, petrographic and geochemical data for these coexisting mafic and felsic suites suggest that their genesis may involve a complex interplay of several petrogenetic processes, including contemporaneous melting of distinct sources and fractional crystallization. To unravel this complex petrogenetic scenario, we attempt here to constrain the source end-members of this mafic–felsic igneous suite.

7.2.1 Gabbro-diorite

In the VBQD, gabbro-dioritic types represent the less evolved rocks. These rocks have geochemical features similar to modern magmatic arc rocks worldwide (e.g., Stern, 2002). Selective enrichment of LILE, U, Pb and LREE, and depletion in HREE and HFSE (e.g., Nb, Ta and Ti) (Table 2), thus resulting in high values of La/Nb

Table 3 SHRIMP U-Th-Pb isotopic data of zircons from the leucogranites of the Val Biandino Intrusive Suite

	ppm					Isotope ratios						Ages (Ma)						
	U	Th	^{206}Pb	±err (%)	Th/U	^{207}Pb/^{206}Pb	±err	^{206}Pb/^{238}U	±err	^{207}Pb/^{235}U	±err	^{207}Pb/^{206}Pb	±err	^{206}Pb/^{238}U	±err	^{207}Pb/^{235}U	±err	% discord
VBQD																		
VBZ3-1.1	627.6	1064.1	23.4	0.2	1.74	0.0518	0.0012	0.0430	0.0008	0.3069	0.0091	276.3	53.2	271.3	4.7	271.8	7.1	-0.2
VBZ3-10.1	208.6	88.0	8.5	1.6	0.43	0.0491	0.0058	0.0462	0.0008	0.3131	0.0375	154.9	255.6	291.1	5.2	276.6	29.4	5.0
VBZ3-11.1	345.7	119.5	13.6	0.0	0.35	0.0514	0.0025	0.0455	0.0007	0.3223	0.0168	259.5	110.0	286.6	4.5	283.7	13.0	1.0
VBZ3-12.1	349.2	317.7	13.3	0.3	0.93	0.0492	0.0014	0.0439	0.0009	0.2980	0.0103	158.9	64.8	277.0	5.4	264.8	8.1	4.4
VBZ3-13.1	596.6	304.7	22.4	0.1	0.52	0.0517	0.0017	0.0433	0.0009	0.3088	0.0121	270.9	73.0	273.5	5.8	273.2	9.4	0.1
VBZ3-14.1	753.3	555.1	29.1	0.2	0.76	0.0517	0.0017	0.0446	0.0005	0.3177	0.0111	272.9	73.0	281.0	3.3	280.1	8.6	0.3
VBZ3-15.1	992.0	842.0	39.2	0.5	0.87	0.0474	0.0011	0.0455	0.0010	0.2974	0.0095	107.2	43.1	286.7	3.1	264.3	6.7	7.8
VBZ3-16.1	400.1	880.4	15.7	0.7	2.26	0.0472	0.0013	0.0450	0.0007	0.2928	0.0096	130.6	32.2	283.5	2.8	260.7	7.5	8.0
VBZ3-17.1	148.3	98.9	5.5	0.4	0.68	0.0496	0.0023	0.0426	0.0008	0.2914	0.0145	175.3	103.0	269.1	5.2	259.6	11.5	3.5
VBZ3-17.2	244.3	190.0	9.4	0.6	0.80	0.0471	0.0015	0.0441	0.0006	0.2911	0.0093	150.0	52.5	278.1	6.8	259.4	14.4	6.7
VBZ3-2.1	994.9	353.2	39.1	0.2	0.36	0.0502	0.0009	0.0452	0.0009	0.3133	0.0089	205.5	43.0	285.3	5.8	276.8	6.9	3.0
VBZ3-3.1	1886.3	992.2	72.1	0.2	0.54	0.0516	0.0004	0.0441	0.0013	0.3137	0.0100	268.3	19.8	278.1	8.3	277.1	7.7	0.4
VBZ3-4.1	255.4	478.4	10.2	0.7	1.92	0.0490	0.0024	0.0458	0.0004	0.3092	0.0156	146.3	112.2	288.6	2.6	273.5	12.2	5.2
VBZ3-6.1	610.1	266.8	24.1	0.4	0.45	0.0509	0.0009	0.0455	0.0016	0.3195	0.0122	237.3	38.4	286.8	9.6	281.5	9.5	1.9
VBZ3-8.1	573.2	793.0	22.5	0.5	1.42	0.0488	0.0014	0.0452	0.0010	0.3041	0.0111	137.5	64.6	285.0	6.5	269.6	8.7	5.4
Inherited cores																		
VBZ3-9.1	1115.0	655.8	46.5	0.3	0.60	0.0495	0.0004	0.0481	0.0009	0.3281	0.0069	172.1	20.4	302.6	5.5	288.1	5.3	4.8
VBZ3-11.2	1102.1	645.3	44.3	0.25	0.59	0.0521	0.0001	0.0482	0.0009	0.3463	0.0065	289.1	6.0	303.6	5.5	301.9	4.9	0.5
VBZ3-21.1	573.8	202.8	43.5	0.1	0.35	0.0593	0.0005	0.0876	0.0010	0.7165	0.0103	579.9	16.8	541.1	6.0	548.6	6.1	-1.4

Table 3 (continued)

	ppm					Isotope ratios						Ages (Ma)						
	U	Th	^{206}Pb	± err (%)	Th/U	^{207}Pb/^{206}Pb	± err	^{206}Pb/^{238}U	± err	^{207}Pb/^{235}U	± err	^{207}Pb/^{206}Pb	± err	^{206}Pb/^{238}U	± err	^{207}Pb/^{235}U	± err	% discord
VBZ3-21.2	1208.7	106.4	88.4	0.2	0.09	0.0589	0.0006	0.0844	0.0015	0.0589	0.0006	4699.8	57.2	522.5	17.0	530.1	16.4	-1.4
VBZ3-22.1	1167.1	819.4	58.7	0.2	0.70	0.0514	0.0004	0.0580	0.0008	0.0514	0.0004	3949.5	48.6	363.5	9.9	349.7	9.6	3.8
VBZ3-23.1	569.3	201.2	44.1	0.1	0.28	0.0589	0.0006	0.0845	0.0015	0.0589	0.0006	4704.5	56.7	522.7	16.9	531.4	16.3	-1.7
VSBG																		
VBZ43-1.1	259.8	97.7	10.0	0.6	0.39	0.0486	0.0019	0.0440	0.0009	0.2953	0.0129	130.1	88.6	277.8	5.3	262.7	10.1	5.4
VBZ43-3.1	300.2	293.2	11.8	0.5	1.00	0.0490	0.0023	0.0453	0.0011	0.3060	0.0164	147.5	108.2	285.6	6.7	271.1	12.8	5.1
VBZ43-5.1	1031.7	400.0	39.6	0.2	0.40	0.0517	0.0007	0.0443	0.0007	0.3158	0.0066	273.7	28.8	279.2	4.4	278.6	5.1	0.2
VBZ43-6.1	930.5	340.5	35.9	0.2	0.38	0.0508	0.0006	0.0445	0.0007	0.3116	0.0064	231.9	28.4	280.6	4.4	275.5	5.0	1.8
VBZ43-1.1	306.8	255.0	12.0	0.1	0.85	0.0527	0.0008	0.0451	0.0007	0.3281	0.0072	317.9	33.2	284.5	4.4	288.1	5.5	1.3
VBZ43-11.1	490.5	143.1	19.0	0.3	0.30	0.0494	0.0011	0.0446	0.0007	0.3038	0.0086	165.5	53.6	281.5	4.3	269.4	6.7	4.3
VBZ43-12.1	197.5	146.1	7.4	0.2	0.76	0.0510	0.0024	0.0433	0.0009	0.3040	0.0157	238.7	104.8	273.1	5.6	269.5	12.3	1.3
VBZ43-13.1	2028.2	392.2	80.6	0.1	0.20	0.0513	0.0006	0.0459	0.0006	0.3245	0.0057	254.1	24.8	289.2	3.7	285.4	4.4	1.3
VBZ43-14.1	431.1	247.8	16.6	0.1	0.59	0.0507	0.0008	0.0445	0.0011	0.3114	0.0092	228.5	37.4	280.8	6.7	275.3	7.2	2.0
VBZ43-15.1	443.4	392.2	16.9	0.4	0.91	0.0502	0.0010	0.0440	0.0008	0.3041	0.0083	202.1	47.6	277.4	4.7	269.6	6.5	2.8
VBZ43-16.1	1298	532	50.3	0.1	0.42	0.0504	0.0008	0.0448	0.0007	0.3112	0.0068	214.3	36.4	282.4	4.1	275.1	5.3	2.6
VBZ43-16.2	1409	386	54.8	0.06	0.28	0.0524	0.0006	0.0449	0.0009	0.3248	0.0073	304.5	26.6	283.3	5.3	285.6	5.6	-0.8
VBZ43-17.1	1023	459	38.9	0.22	0.46	0.0501	0.0007	0.0439	0.0006	0.3032	0.0059	200.5	30.8	276.8	3.7	268.9	4.6	2.9
VBZ43-19.1	392	157	15.6	0.16	0.41	0.0505	0.0015	0.0459	0.0007	0.3194	0.0104	216.3	65.6	289.3	4.1	281.4	8.0	2.7
VBZ43-2.1	445	233	17.6	0.51	0.54	0.0492	0.0016	0.0456	0.0007	0.2971	0.0112	156.3	67.2	287.2	4.4	264.1	8.8	8.0

Table 3 (continued)

	ppm					Isotope ratios						Ages (Ma)						
	U	Th	^{206}Pb	±err (%)	Th/U	^{207}Pb/^{206}Pb	±err	^{206}Pb/^{238}U	±err	^{207}Pb/^{235}U	±err	^{207}Pb/^{206}Pb	±err	^{206}Pb/^{238}U	±err	^{207}Pb/^{235}U	±err	% discord
VBZ43-3.1	431	216	16.3	0.22	0.52	0.0493	0.0009	0.0437	0.0017	0.2966	0.0131	159.7	43.4	275.6	10.8	263.8	10.3	4.3
VBZ43-4.1	602	292	24.1	0.29	0.50	0.0482	0.0006	0.0461	0.0006	0.3062	0.0060	110.3	31.0	290.2	4.0	271.2	4.7	6.5
VBZ43-5.1	502	249	20.0	0.35	0.51	0.0487	0.0015	0.0458	0.0012	0.3073	0.0122	131.5	69.0	288.7	7.3	272.1	9.5	5.8
VBZ43-8.1	1303	550	49.0	0.22	0.43	0.0497	0.0007	0.0434	0.0008	0.2975	0.0073	182.3	33.2	273.8	5.2	264.5	5.7	3.4
VBZ43-9.1	267	255	10.1	0.58	0.98	0.0493	0.0026	0.0435	0.0007	0.2956	0.0161	160.3	117.6	274.6	4.2	262.9	12.7	4.2
VBZ43-9.2	467	219	17.9	0.0	0.48	0.0519	0.0011	0.0443	0.0008	0.3173	0.0088	281.5	47.8	279.6	4.8	279.9	6.8	-0.1

	U (ppm)	Th (ppm)	% from ^{204}Pb	±err (%)	Th/U	^{207}Pb/^{206}Pb	±err	^{206}Pb/^{238}U	±err	^{207}Pb/^{206}Pb	±err	^{206}Pb/^{238}U	±err
TEMORA													
TEM-1.1	262.5	70.4	0.84	0.02	0.28	2.1355	0.0563	0.6945	0.1067	165.5	36.8	418.1	3.0
TEM-2.1	235.9	67.0	0.51	0.10	0.29	2.0391	0.0553	1.4843	0.1070	245.5	29.9	417.4	3.4
TEM-5.1	160.8	36.4	0.62	0.11	0.23	2.4099	0.0573	2.3930	0.1205	299.2	34.9	426.2	9.1
TEM-8.1	398.7	184.8	0.24	0.03	0.48	1.6014	0.0550	0.5901	0.1075	331.7	14.1	416.8	2.7
TEM-9.1	592.5	171.6	0.13	0.05	0.30	1.3059	0.0553	1.7092	0.1102	378.3	8.1	418.4	4.3
TEM-10.1	250.5	117.6	0.46	0.06	0.49	2.0190	0.0561	0.7221	0.1119	302.9	25.6	412.6	3.1
TEM-11.1	227.8	101.5	0.70	0.03	0.46	2.0372	0.0560	2.8517	0.1174	209.9	35.4	418.1	7.7
TEM-12.1	156.7	71.9	0.58	0.10	0.47	2.4020	0.0581	0.8733	0.1083	345.7	33.6	412.2	3.7
TEM-15.1	679.0	333.2	0.28	0.04	0.51	1.2357	0.0553	2.5138	0.1112	328.9	12.7	421.5	2.1
TEM-16.1	314.3	110.2	0.35	0.04	0.36	1.7797	0.0560	1.4767	0.1091	334.4	19.1	417.4	2.8
TEM-18.1	342.4	165.1	0.27	0.05	0.50	1.7338	0.0560	1.5885	0.1141	362.7	15.1	412.1	3.0
TEM-20.1	157.4	46.2	0.47	0.11	0.30	2.5788	0.0550	2.2773	0.1102	251.0	34.9	412.2	4.3
TEM-23.1	465.4	106.1	0.23	0.21	0.24	1.4551	0.0546	1.5601	0.1095	317.3	12.5	415.1	4.8
TEM-24.1	626.5	238.0	0.19	0.52	0.39	1.2358	0.0546	2.3623	0.1072	329.0	10.2	417.2	1.9

Errors are at one sigma level. U, Th and ^{206}Pb contents are expressed in ppm. The error in 206/238 averaging the standard has been already propagated. Th/U ratios are atomic (232/238), not in weight

Point-to point errors, calculated on replicates of the TEMORA standard, are: 0.39% for ^{206}Pb/^{238}U, and 0.31% for ^{207}Pb/^{206}Pb

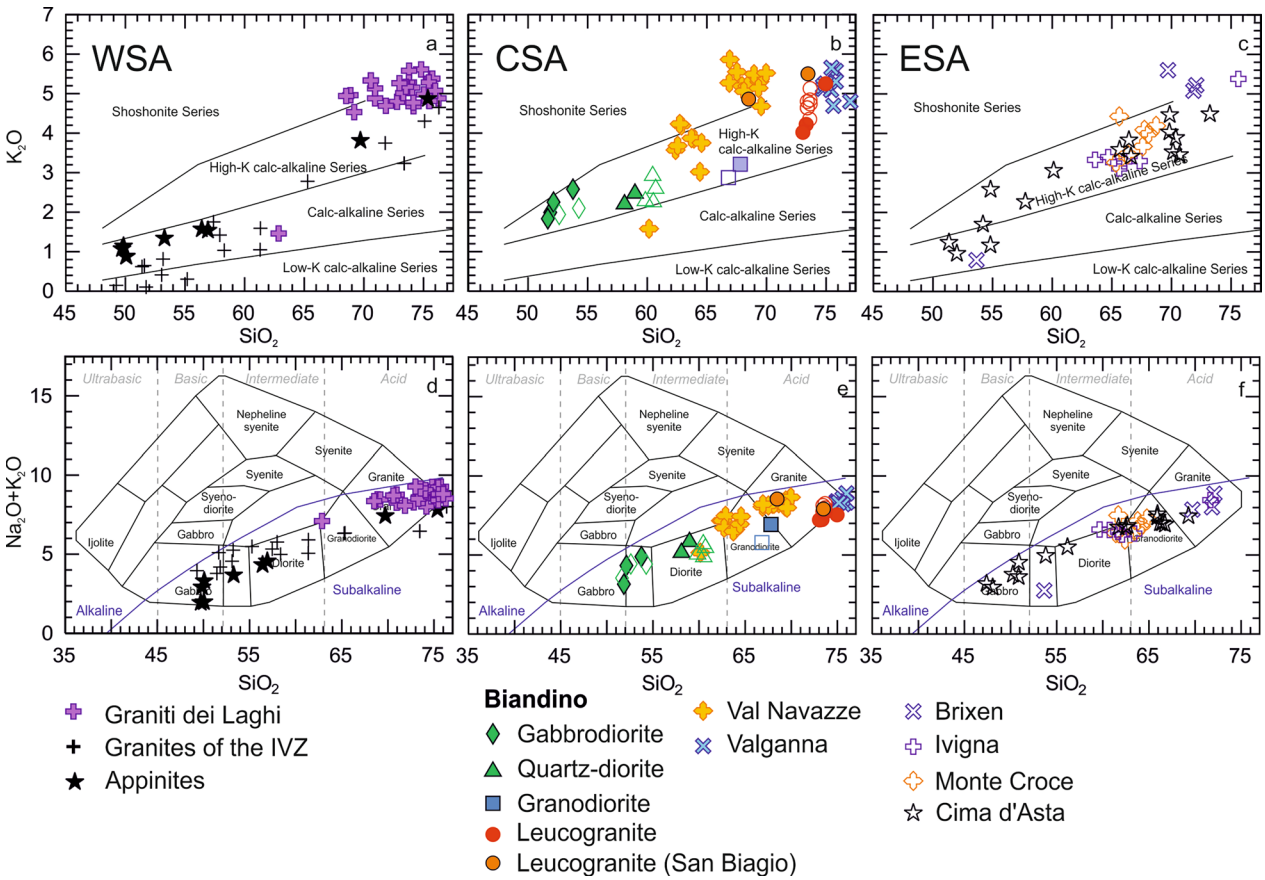

Fig. 11 Whole rock data of the major intrusive bodies of Early Permian age in the western (WSA, **a** and **d**), central (CSA, **b** and **e**) and eastern southern Alps (ESA, **c** and **f**). All intrusive bodies are subalkaline with a calc-alkaline affinity. Rocks from the CSA and ESA, independently from their SiO_2 content, are always high in K_2O, whereas in the WSA more mafic terms are strictly calc-alkaline or even low-K calc-alkaline

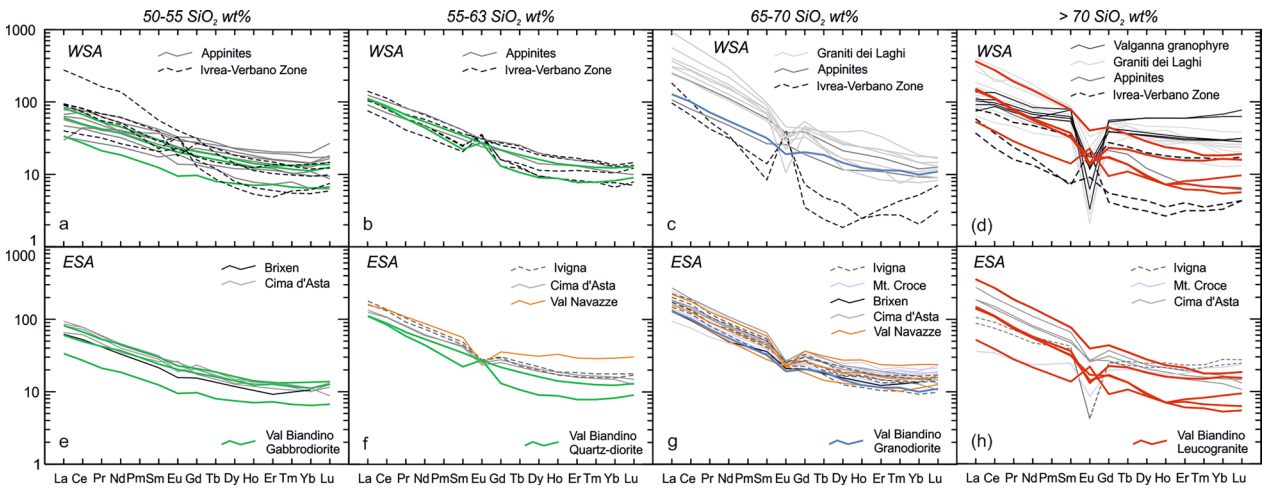

Fig. 12 Chondrite normalized (McDonough and Sun, 1995) REE pattern of Early Permian intrusive rocks from the western (WSA), central (CSA) and eastern Southern Alps (ESA). Intrusive rocks in the central Southern Alps are basically represented by the Val Biandino Intrusive Complex and the Val Navazze Complex: their REE patterns (in colour) are compared in the diagrams with both the WSA and ESA intrusives having the same SiO_2 content

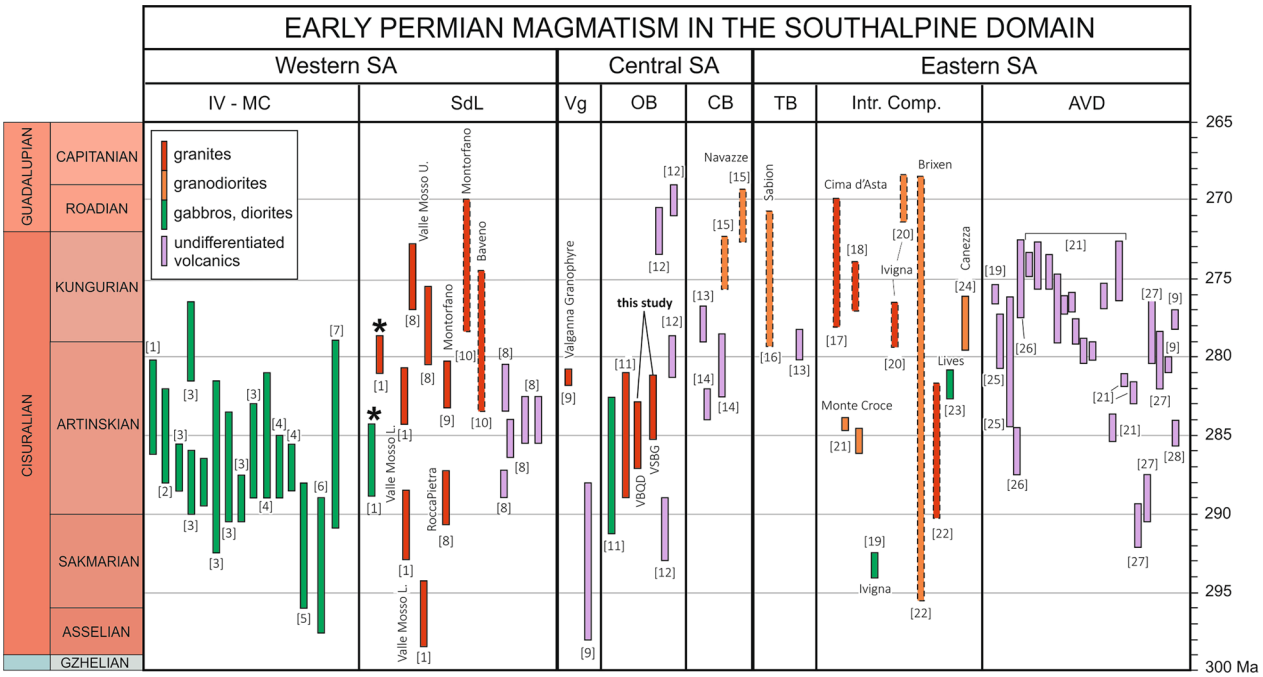

Fig. 13 Compilation of available radiometric ages related to the Early Permian magmatic activity in the Southalpine domain. Age of volcanic rocks have been also included. IV-MC: Ivrea-Verbano Mafic Complex; SdL: "Serie dei Laghi" granodiorites and granites; Vg: Valganna granophyre; OB: Orobic Basin; CB: Collio Basin; TB: Tregiovo Basin; Intr.Comp.: intrusive complex in the ESA (Monte Croce, Ivigna and Bressanone); AVD: Athesian Volcanic District. Bars with dashed outline refers to low-retentivity isotopic systems (mainly Rb–Sr whole rock or mica ages); bars with continuous outline are U–Pb zircon ages. [1] Klötzli et al., 2014; [2] Sinigoi et al., 2011; [3] Peressini et al., 2007; [4] Quick et al., 2003; [5] Garuti et al., 2001; [6] Vavra et al., 1999; [7] Quick et al., 2009; [8] Schaltegger & Brack, 2007; [9] Pinarelli et al., 1988; [10] Berra et al., 2015; [11] Gretter et al., 2013; [12] Schaltegger & Brack, 1999; [13] De Capitani et al., 1994; [14] Borsi et al., 1966; [15] Macera et al., 1994; [16] Barth et al., 1993; [17] Morelli et al., 2012; [18] Marocchi et al., 2008; [19] Rottura et al., 1998; [20] Del Moro & Visonà, 1982; [21] Avanzini et al., 2010; [22] Bargossi et al., 2010; [23] Klötzli et al., 2003

(ca. 3), Ba/Nb (43–53), Ba/La (>15) and Zr/Nb ratios (10–22) and low Ce/Pb (3.6–8.9) (Table 2). The gabbro-diorite has an initial $^{87}Sr/^{86}Sr$ value of 0.70853 (Fig. 14, data from Thöni et al., 1992; De Capitani et al., 1994; all $^{87}Sr/^{86}Sr$ values reported hereafter for the Val Biandino Intrusive Suite have been recalculated at 290 Ma) higher than those of E-MORB and Hawaiian ocean island basalts (e.g., Saunders et al., 1980). Such geochemical features can be ascribed either to partial melting of a metasomatized mantle source enriched in LILE and LREE by slab-derived hydrous fluids or melts or to crustal contamination of a MORB-like magma during its emplacement.

Any mantle-derived magmas passing through a thick crustal section should interact with it, resulting in some degrees of contamination/assimilation (Hawkesworth et al., 1984; Mahoney, 1988; Carlson, 1991; Hergt et al., 1991). Actually, a simple process of binary mixing cannot explain the compositional features of the gabbro-diorite suite. The lack of a granite end-member associated with the gabbro-diorite makes the mixing hypothesis unfeasible for this suite. The gabbro-diorite have higher Sr abundance (224–244 ppm) and distinct Sr isotopic composition ($(^{87}Sr/^{86}Sr)=0.70853$) with respect to those of the local upper crust host rocks (Sr = 84–180 ppm; $(^{87}Sr/^{86}Sr)=0.712–0.718$) as represented by the metasediments of the Orobic basement (Fig. 14, Sr isotopic ratios recalculated at 290 Ma). This argues against such basement as the potential source of the enrichments observed in the gabbro-diorite suite.

If crustal assimilation for the gabbro-diorites can be excluded, source contamination must be considered as a main factor in their petrogenesis. In the Nb/Ba vs. Nb/Zr diagram (Fig. 15a; e.g., Hooper & Hawkesworth, 1993), gabbro-diorites plot close to the field for subcontinental lithospheric mantle and far away from oceanic island basalt and E-MORB sources. Zr/Ba (0.15–0.4) and Nb/La (<0.5) values also support a subcontinental lithospheric mantle as source region for the gabbro-dioritic melt. For the transport of trace elements in the mantle wedge, the prevailing model is that different types of metasomatic agents (e.g., fluid, silicic or carbonatite melt) could yield distinctive trace elements and isotopic imprints in a metasomatized mantle (e.g., Menzies et al., 1987). For instance, slab-derived fluids usually carry significant amounts of Si and LILE in the mantle wedge at shallow depths (e.g., Plank and Langmuir, 1993; Stein et al., 1997),

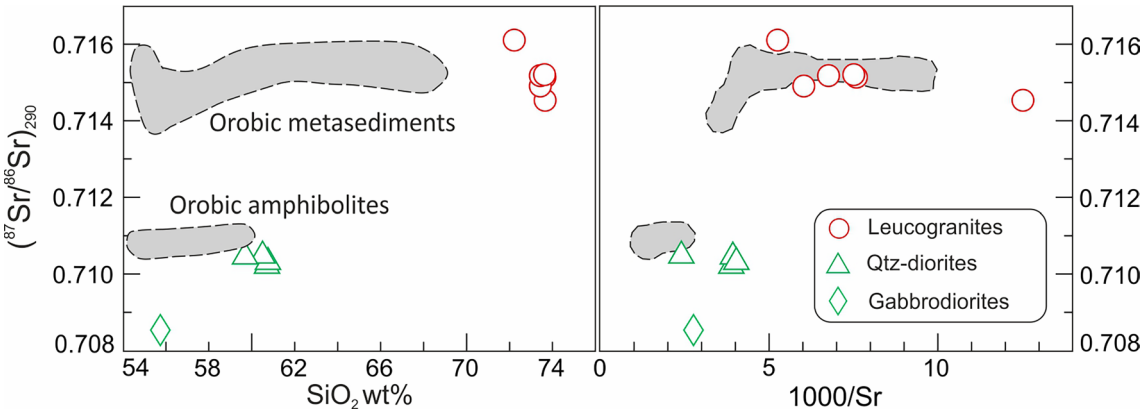

Fig. 14 $^{87}Sr/^{86}Sr_i$ isotopic composition of the VBQD (Thöni et al., 1992) compared with the rocks (metasediments and amphibolites) of the Orobic Variscan basement (Boriani et al., 2003) plotted against SiO_2 wt% (**a**) and 1000/Sr (**b**), respectively. The $^{87}Sr/^{86}Sr$ ratio has been recalculated at 290 Ma

whereas slab melts may be the metasomatic agents at greater depths (Kilian and Stern, 2002; Rapp et al., 1999) and produce more sodic metasomatic products. Sun & Stern (2001) used Ba/La, Pb/Ce, Cs/Rb and U/Th ratios to identify fluid enriched sources. These ratios are > 1, which means that magmas derived from fluid-metasomatized sources are enriched in Ba, Pb, Cs and U relative to La, Ce, Rb and Th, respectively. Woodhead et al. (1998) suggested that if the mantle is enriched by melts from subducted sediments, it would be reflected in the Th/Yb ratio in mafic magmas. Consequently, these variables can be used as reliable indicators of potential sediment or fluid contributions from the subducted slab to magma source regions (Woodhead, et al., 2001). Based on mass

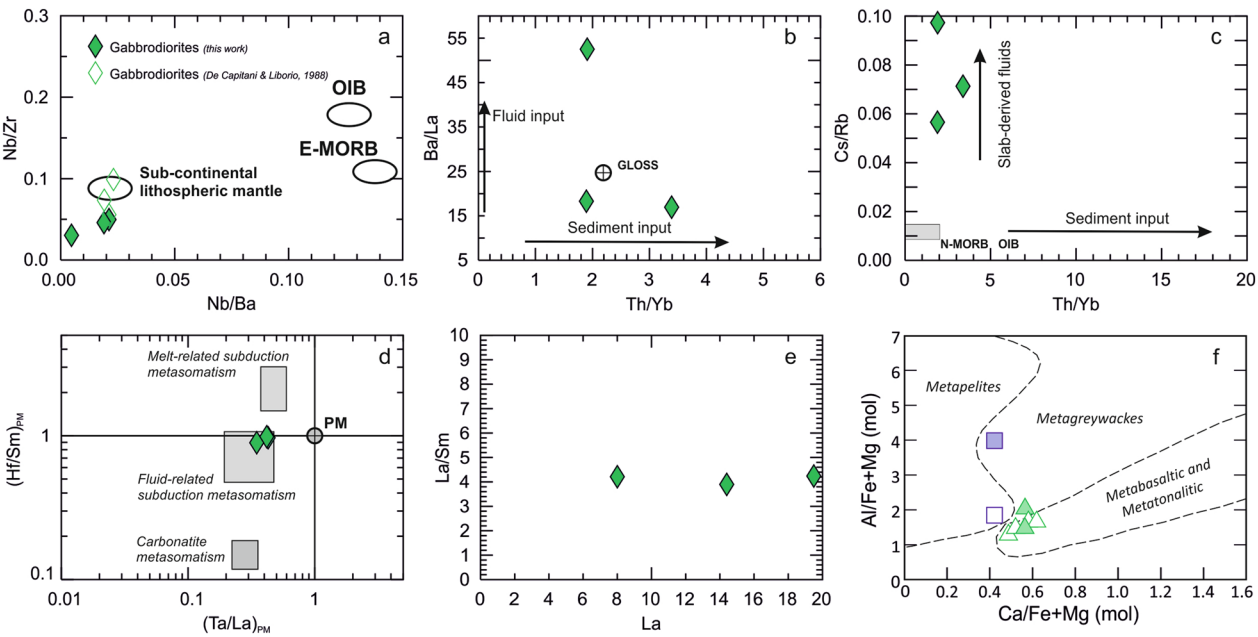

Fig. 15 **a** The Nb content of the mafic rock types of the VBQD with respect to Zr and Ba (Nb/Ba vs. Nb/Zr diagram of Hooper & Hawkesworth, 1993). Data from this work and literature (De Capitani & Liborio, 1988) show how a sub-continental lithospheric mantle is favourable as a source for the VBQD magmatic rocks. **b** Th/Yb – Ba/La, **c** Th/Yb – Cs/Rb and **d** $(Ta/La)_{PM}$ – $(Hf/Sm)_{PM}$ diagrams (Hartmann & Wedepohl, 1993) that show the sediments and fluids possible contribution to the source of the Biandino gabbrodiorites. **e** A simple fractionation mechanism of magma derived from a fluid- and/or melt-metasomatized subcontinental lithospheric mantle is supported by the incompatible trace element ratios (Soesoo, 2000) and by the fractional crystallization tendency depicted in the La/Sm vs La diagram for gabbrodiorite of the VBQD. **f** Relationships between the composition of anatectic melt with respect of the source composition in terms of the Ca/Fe + Mg and Al/Fe + Mg molar ratios (Altherr et al., 2000). The composition of quartz-diorite and granodiorite of the VBQD suggest a contribution derived from partial melting of metapelites-metapsammites (micaschists and paragneisses) and metamorphic mafic rocks (amphibolites) for quartz-diorite

balance considerations, Hawkesworth et al. (1995) suggested that the elevated Ba/La and La/Nb in mafic rocks from the Basin and Range province (USA) cannot realistically be attributed to crustal contamination of MORB-type magmas, and that such rocks are connected to metasomatized source regions in the subcontinental lithospheric mantle. In our case, high Ba content and Th/Yb, La/Nb, Ba/La, (Hf/Sm)PM and Cs/Rb and low (Ta/La)PM ratios point to a mantle source region enriched by both fluids and sediments from a subducting slab (Fig. 15b–d). The high Ba (ca. 400 ppm) content and Ba/Ce (ca. 10) ratios, along with the poorly fractionated REE patterns [(La/Yb)N = 5–6)] suggest a shallow H_2O-metasomatized mantle (e.g. Hartmann & Wedepohl, 1993) containing hydrous phases like amphibole and phlogopite (as suggested by the high Ba contents; O'Brien et al., 1995) as the source for the gabbro-dioritic melt. H_2O-dominated slab-derived fluids could explain mantle enrichment in mainly LILE (and lesser LREE; Fig. 9f–h), whereas high $^{87}Sr/^{86}Sr$ (0.70853) (Fig. 14) may indicate a significant contribution of continental terrigenous components in the source (Thirlwall et al., 1996), as also recorded in the Neogene calc-alkaline and K-rich volcanics occurring in the Betic Cordillera ($^{87}Sr/^{86}Sr = 0.70874–0.72073$; Zeck et al., 1998; Benito et al., 1999; Turner et al., 1999), in mantle xenoliths from the M. Vulture (S-Italy; e.g., Downes et al., 2002) and in the Finero peridotite (NW-Italy; e.g., Obermiller, 1994).

In summary, the available data are not compatible with a magma mixing at the level of emplacement as mechanism that yielded the chemical variations in the gabbro-dioritic suite. A simple fractionation mechanism of magma derived from a fluid- and/or melt- metasomatized subcontinental lithospheric mantle is supported by the incompatible trace element ratios (Soesoo, 2000) and by the fractional crystallization tendency depicted in the La/Sm vs La diagram (Fig. 15e). The absence of positive or negative correlation of La content with LREE fractionation (La/Sm) suggests a simple crystal fractionation process with highly incompatible elements (La) not enriched with respect to less incompatible ones (Sm). Other processes, like partial melting or different degree of crustal contamination, should have resulted in different patterns (Aldanmaz et al., 2000).

7.2.2 Quartz-diorite and granodiorite

The quartz-diorite and granodiorite have different trace element concentrations compared to the gabbro-diorites (Fig. 9), precluding a single partial melting/fractionation/assimilation model for these rocks. If this had happened close similarities in trace element abundances and patter should be expected at least for the gabbro-diorite and the quartz-diorite. In addition, the difference in Sr isotope compositions rules out a direct derivation of the quartz-diorites from the gabbro-diorites (Fig. 14) as they differ of ca. 0.02 in $^{87}Sr/^{86}Sr$, recalculated at 290 Ma (Fig. 14).

The low concentrations of Ni and Cr (Table 2) argue against a pure mantle derivation of the quartz-diorite, even though similar low abundances have been reported in the least evolved members of some arc-type and calc-alkaline series (e.g., Perfit et al., 1980). Some trace element characteristics are typical for arc-like magmatism: enrichment of LILE (Ba, Rb, K), relative depletion of HFSE (e.g. Nb) and, consequently, high LILE/HFSE ratios (Fig. 9). Transfer of volatiles might cause enrichment in LILE from dehydrating subducted oceanic crust to the mantle wedge (e.g., Hawkesworth, 1979; Hawkesworth & Vollmer, 1979; Thirlwall & Graham 1984). In the absence of a subduction zone setting, enrichment of LILE may be caused by preferential tapping of enriched mantle sources (e.g., Saunders et al., 1980) or may be caused by AFC (assimilation-fractional crystallization) or MASH (melting–assimilation–storage–homogenization) processes (e.g., Hildreth & Moorbath 1988). The less evolved quartz-diorite samples have high $^{87}Sr/^{86}Sr$ values (0.7104; Thöni et al., 1992; Fig. 14). While large-scale crustal contamination of magma derived from upper mantle sources could explain the Sr isotopic composition, such contamination would likely be accompanied by strong fractional crystallization, which is not observed (Fig. 9), as granodiorite display almost the same trace element abundances of more mafic terms. These features likely exclude a significant involvement of mantle-derived melts in the genesis of the quartz-dioritic—granodioritic suite.

Compositional differences of granitic liquids produced by partial melting of various sources under variable melting conditions can be distinguished in terms of molar $CaO/(MgO + FeO^*)$ vs. molar $Al_2O_3/(MgO + FeO^*)$ (Fig. 15f; Altherr et al., 2000). The dominant mafic composition of the quartz-diorites precludes partial melting of metasedimentary or felsic meta-igneous rocks, with partial melting of mafic to intermediate sources that seems necessary in order to explain the major and trace element contents. Experimental evidence (Beard & Lofgren, 1989, 1991; Rapp et al., 1991; Rushmer, 1991; Wolf & Wyllie, 1994; Rapp & Watson, 1995; Sisson et al., 2005) suggests that dehydrating basaltic material within the mid- to lower crust can produce significant volumes of mafic to intermediate partial melts, particularly in regions characterized by high heat flow. These studies have shown that melting conditions (water-saturated vs. dehydration melting, water fugacity etc.) strongly influence the composition of the melt and of the residuum during partial melting of rocks of basaltic compositions at mid- to lower crustal pressures (e.g., Beard and Lofgren 1989, 1991; Wolf and Wyllie 1989; Sisson et al., 2005).

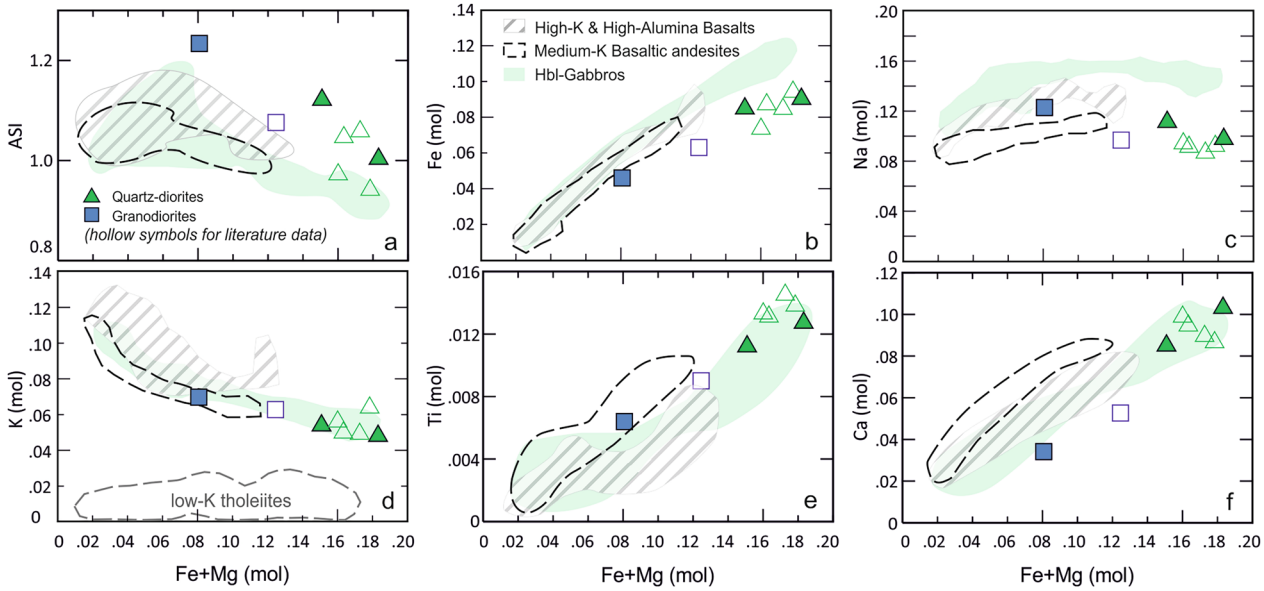

Fig. 16 Composition of the VBQD high-K calc-alkaline rocks compared to the compositions of melts experimentally generated by partial melting of high-K Hbl-gabbros, basalts and basaltic andesites (Sisson et al., 2005)

Depending on bulk composition, fluid-absent melting of amphibolite yields 10 – 60% of melt at temperatures of 900–1000 °C, whereas fluid-present melting yields similar amounts of melt at lower temperatures between 850 and 900 °C (e.g., Beard & Lofgren 1991; Rushmer 1991; Wolf & Wyllie 1994; Sisson et al., 2005). However, liquids produced experimentally by fluid-absent melting are quartz-dioritic to tonalitic in composition and coexist with a residuum dominated by plagioclase, pyroxene and Fe-Ti oxides (Beard & Lofgren 1991; Rushmer 1991; Wolf & Wyllie 1994), whereas melts generated in the presence of an H_2O-rich fluid phase are "granitic" in composition (rich in SiO_2 and Al_2O_3 and low in Fe_2O_3 and MgO) and coexist with a residuum of amphibole, clinopyroxene, Fe-Ti oxides and minor plagioclase (Beard & Lofgren 1991).

The most primitive quartz-diorite (SiO_2 = 58 wt%) of the Val Biandino Intrusive Suite has chemical features recalling melts derived from a mafic source: moderately high Al_2O_3 (17.5 wt%), MgO (3.7 wt%), FeO* (6.3 wt%), K_2O (2.2 wt%) and Na_2O (2.94 wt%) contents and Na_2O/K_2O (> 1.3) ratio, high LREE (118 ppm) and moderately low HREE (15 ppm) concentrations, and no Eu anomaly (Eu/Eu* ca. 1) (Fig. 9; Table 2). Moreover, it does not show significant HREE depletion (i.e. $Yb_N < 10$; Wareham et al., 1997) predicted for melts that equilibrated with residual garnet, suggesting that it formed alternatively under lower pressures. Also, its REE pattern is akin to models involving partial melting of an amphibolitic source (Arth & Barker, 1976; Arth et al., 1978; Sengupta et al., 1983). The patterns show in Fig. 9 with the decreasing of ΣREE and increasing of positive anomaly are very similar to ones expected if hornblende fractionation was operating to produce the melt.

Since melts derived from fluid-absent experiments on partial melting of a mafic source (e.g. Rapp et al., 1991) are generally too sodic in composition to justify the formation of medium- to high-K granitoids, Sisson et al. (2005) suggested that metaluminous to weakly peraluminous K_2O-enriched granitoids may derive from fluid-absent partial melting of medium- to high-K Hbl-gabbros, basalts and basaltic andesites (Fig. 16). Although experimental melts obtained at 925–1000 °C and ca. 7 kbar (Sisson et al., 2005) have produced melts having chemical composition comparable to those of the quartz-diorites and granodiorites in terms of Al, Ca and K contents (Fig. 16), some chemical signatures argue against this interpretation. Partial melting of these source rocks produces melts that have higher Fe and Na and lower Mg and Ti concentrations than the quartz-dioritic–granodioritic suite (Fig. 16). Moreover, partial melting of Hbl-gabbro, basalt and basaltic andesites produces melts that are only slightly peraluminous, while some of the samples of the quartz-diorite–granodioritic suite of the Val Biandino Intrusive Suite display higher ASI (Fig. 16a). In addition, the $^{87}Sr/^{86}Sr$ isotopic composition (0.7102–0.7105; Fig. 14) of the quartz-dioritic–granodioritic suite has a strong crustal signature excluding their derivation from a typical basaltic source.

The K/Na ratios (0.5–0.7) that characterize the quartz-dioritic–granodioritic suite indicate that biotite could be a reactant phase in the melting reaction, thus suggesting that the source underwent concomitant biotite and amphibole incongruent melting. Fluid-absent melting of these two phases produces both peritectic clinopyroxene and orthopyroxene, with the two pyroxenes that, at low pressures, may also be intergrown (Skjerlie & Johnston, 1996). The positive linear correlation for Ti and Ca plotted against Fe + Mg (mol) (Fig. 16e, f) together with the negative correlation of ASI (Fig. 16a) suggests the entrainment in the source of a peritectic assemblage dominated by a Ca–Fe–Mg–Ti bearing phase or assemblage of phases. The entrainment of both peritectic clinopyroxene and ilmenite phases (e.g., Vielzeuf & Montel, 1994) in the magma can generate the chemical variability exhibited by the quartz-dioritic–granodioritic suite. The entrainment of clinopyroxene can be responsible for the positive correlation of Ca and Mg and the negative one of ASI with Fe + Mg, whereas the entrainment of ilmenite can explain the increase in Ti (Fig. 16e). The entrainment of peritectic ilmenite is also supported by the positive correlation that exists between TiO_2 and V for the rocks of the quartz-dioritic–granodioritic suite (Table 2). In the quartz-diorite mineral phases that may represent remnants of a peritectic assemblage could be the aggregates of amphiboles that in many calc-alkaline granitic rocks have been described (e.g. Castro and Stephens, 1992; Sial et al., 1998) as fragments of "restites" modified in response to the increase of water activity in the melt during crystallization (Stephens, 2001).

The formation of a peraluminous melt in equilibrium with a clinopyroxene-dominated peritectic assemblage provides constraints on the nature of the source and argues for concurrent biotite and amphibole fluid-absent melting in the genesis of the quartz-dioritic–granodioritic suite. Few experiments have been performed on source rocks containing multiple hydrous phases (Rutter & Wyllie, 1988; Skjerlie & Johnston, 1992, 1996; Skjerlie & Patiño Douce, 1995). Granitic melt and clinopyroxene-dominated peritectic assemblage are produced by partial melting of: (i) immature volcanogenic sediments of andesitic-dacitic composition (e.g., Skjerlie & Johnston, 1996) or potassic arc andesites (Roberts and Clemens, 1993); (ii) interlayered garnet-bearing amphibolites and sillimanite-bearing metapelite (Skjerlie & Patiño Douce, 1995). These sources are able to produce 20–60 vol.% of melt at temperatures of ca. 900 °C while, according to Thompson (2001), metavolcanics containing low-Ca amphiboles and biotite can undergo substantial fluid-absent melting at lower temperatures (T ca. 825 °C). It is important to emphasize that rocks similar to those used as starting material in the experiments of Skjerlie & Patiño Douce (1995) occur in the Paleozoic Orobic basement (Boriani et al., 2012), which is made up of metapelites and metapsammites ("Orobic metasediments" in Fig. 14) interlayered with minor quartzites and lenses of amphibolites ("Orobic amphibolites" in Fig. 14). These latter mainly consist of plagioclase, hornblende and biotite, and their protholiths is interpreted as a basaltic meta-tuffite (Boriani et al., 2003). Finally, the chemical differences between the quartz-diorite and granodiorite may be the effect of temperature increase in a biotite and hornblende-bearing source. However, the origin of granodiorite from partial melting of a metasedimentary source unrelated to the source of the quartz-diorite can not be ruled out.

7.2.3 Leucogranite

Peraluminous granites and leucogranite occurs in the studied area as small stocks and dikes in the VBQD and form almost the entire body of the VSBG. Granites in the VBQD always contain muscovite together with cordierite in most of them. As determined by U–Pb zircon dating (Fig. 10), granites in the two complexes are almost coeval considering uncertainties.

Aluminous silicate minerals, such as cordierite, and muscovite are characteristic minerals of S-type granitoids (e.g., Chappell & White, 2001) suggesting that the granites of the Val Biandino Intrusive Suite most likely have a metasedimentary source (Miller, 1985), also supported by their enrichment of Ba and Rb relative to Sr, high K_2O (> 4.0 wt%, Fig. 9) and moderately low CaO (< 2.0 wt%, Table 2) contents, high initial $^{87}Sr/^{86}Sr$ (0.7145–0.7161; Thöni et al., 1992; Fig. 14) and strongly peraluminous character (ASI > 1.2; Table 2). Cordierite is a low-pressure mineral that appears above the granite solidus in many peraluminous felsic magmas (Clarke, 1995), whose occurrence is typical of low-pressure, high-temperature terranes that underwent extensive crustal melting either in the late thermal stages of continental collision or in the high thermal regime during crustal thinning.

Felsic peraluminous melts, such as the cordierite granite, likely form in response of partial melting of metapelites and metapsammites under fluid-absent (Tompson, 1982; Miller, 1985; Breton & Thompson, 1988; Vielzeuf & Holloway, 1988; Vielzeuf et al., 1990; Vielzeuf & Montel, 1994; Patiño Douce & Harris, 1998) or even dry conditions (e.g., White & Chappell, 1977; Miller, 1985; Clemens & Wall, 1981; Turpin et al., 1990; Holtz & Johannes, 1991). The critical parameters controlling formation of cordierite in magmas are relatively low pressure, and high ($Mg + Fe^{2+}$), Mg/Fe^{2+}, ASI, Al_2O_3 activity and fO_2 (Clarke, 1995). Two important fluid-absent melting reactions relevant for the formation of S-type granites at high

temperature (800–900 °C) are (Breton & Thompson 1988; Vielzeuf & Holloway 1988; Vielzeuf & Montel 1994):

(i) Bt + Sil + Qz + Pg = melt + Crd + Grt ± Kfs;
(ii) Bt + Qz + Pg = me lt + Opx ± Grt ± Kfs

At high temperatures (> 800 °C), considerably high degrees of melting (20–40%) are normally associated with these biotite breakdown reactions (Clemens & Vielzeuf 1987; Stevens et al., 1997). Since muscovite is expected to have completely disappeared at lower temperatures during anatexis of metasedimentary rocks, the concentrations of Sr, Ba and Rb are related to the amounts of feldspar and biotite remaining in the residue. The composition of the restite depends, among other factors, on the presence of H_2O-rich fluids during melting: the more H_2O-rich fluid is available, the larger is the proportion of melt that can be formed, and the smaller the proportion of feldspar that remains in the restite (e.g., Harris & Inger, 1992.; Harris et al., 1995; Inger & Harris, 1993). The cordierite granites have Sr = 82–229 ppm, Ba = 405–574 ppm and Rb = 161–237 ppm (Table 2), resulting in low Rb/Sr (0.7–3.0), Rb/Ba (0.3–0.6) and Sr/Ba (0.2–0.3) ratios that recall a (meta)psammitic source rock (Fig. 17c). This distinction probably reflects the higher Rb/Sr and Rb/Ba ratios of clay-rich sources as compared to clay-poor ones. For instance, the average shale has higher Rb/Sr and Rb/Ba than does the average greywacke (Condie, 1993). The wide ranges of Rb and Sr concentrations in our cordierite granites suggest variable proportions of feldspar and biotite remaining in the source during anatexis. Sylvester (1998) suggested that CaO/Na_2O ratio is mainly controlled by the abundance of plagioclase relative to clay within the sedimentary sources. Strongly peraluminous granitic melts produced from plagioclase-rich and clay-poor sources will tend to have higher CaO/Na_2O (> 0.3) ratios than melts derived from sources that are plagioclase-poor and clay-rich (Skjerlie & Johnston, 1996). The CaO/Na_2O ratios of the cordierite granites are 0.3 – 0.6 (Fig. 17a), in further agreement with the conclusion obtained from the Rb/Sr and Rb/Ba ratios. Plots of Ba versus Pb concentrations in S-type granitic rocks have been used to distinguish between those magmas produced by relatively low-temperature partial melting involving muscovite breakdown and those formed by higher-temperature reactions involving biotite breakdown (Finger & Schiller, 2012). A Pb–Ba diagram (Fig. 17b) for the cordierite granite shows that, as expected, all samples plot in the high-temperature field, also in agreement with the low Al_2O_3/TiO_2 ratios (< 100) (Sylvester, 1998). The cordierite bearing granites of the Val Biandino Intrusive Suite fall within the same Pb–Ba field of Variscan S-type granites, interpreted to had formed by high-T crustal anatexis (Finger & Schiller, 2012).

Moreover, the displayed horizontal data spread, can be interpreted as a source-controlled pattern (Finger & Schiller, 2012). The preservation of source-controlled chemical variations implies that the magmatic system was not or only poorly homogenized during its magmatic evolution.

The high-T and H_2O-undersaturated S-type magma that of the cordierite granites could be derived through fluid-absent partial melting (mainly biotite breakdown) of a metapsammite. A possible metasedimentary source could be represented by low- to medium- grade paragneisses and micaschists of the Orobic basement, which are commonly characterized by 55–68 wt% SiO_2, 15–24 wt% Al_2O_3, 2–4 wt% MgO, 3–5 wt% K_2O and 2–4 wt% Na_2O (Boriani et al., 2003). Moreover, their initial Sr isotope ratios recalculated at 290 Ma (0.71155 – 0.7155, Fig. 14; Boriani et al., 2003) are similar to those of the cordierite granite (0.7145–0.7161; Fig. 14; Thöni et al., 1992). This interpretation is also supported by the Rb, Ba and Sr contents. Because Sr and Ba are compatible in plagioclase, whereas Rb is incompatible (e.g. Harris & Inger, 1992), cordierite granites should have higher Rb/Sr (0.7–3) and Rb/Ba (0.3–0.6) than their metapsammitic source (0.3–1.2. and 0.1–0.3, respectively; Boriani et al., 2003). These geochemical features, and the large number of schists enclaves found in the cordierite granites (Fig. 6b) are consistent with an important contribution from a relatively mature metasedimentary source similar to the low- to medium-grade paragneisses and micaschists of the Orobic basement.

Some samples display a positive Eu anomaly that can be explained by fluid-present incongruent melting of muscovite from a metaspammitic source (Fig. 17), in which the depletion of feldspar in the restite would lead to positive Eu anomaly and Sr enrichment in the melt under disequilibrium conditions (Harris & Inger, 1992).

The VSBG granite has major element composition similar to those defined by some experimental melts on metasedimentary sources (Thompson, 1982; Miller, 1985; Breton & Thompson, 1988; Vielzeuf & Holloway, 1988; Vielzeuf et al., 1990; Vielzeuf & Montel, 1994; Patiño Douce & Harris, 1998) (Fig. 17d). The low Rb/Sr, Rb/Ba and high CaO/Na_2O ratios suggest for the VSBG granite a melt derived from a metapsammitic source (Fig. 17a), as for the VBQD cordierite granite. However, some differences can be observed. The VSBG granite show lower MgO, Al_2O_3, Na_2O, and Sr and higher K_2O, FeO*, HREE, and Y values than the cordierite granite (Fig. 9). The higher HREE and Y (without modifying LREE, Fig. 9) contents could indicate the entrainment of peritectic

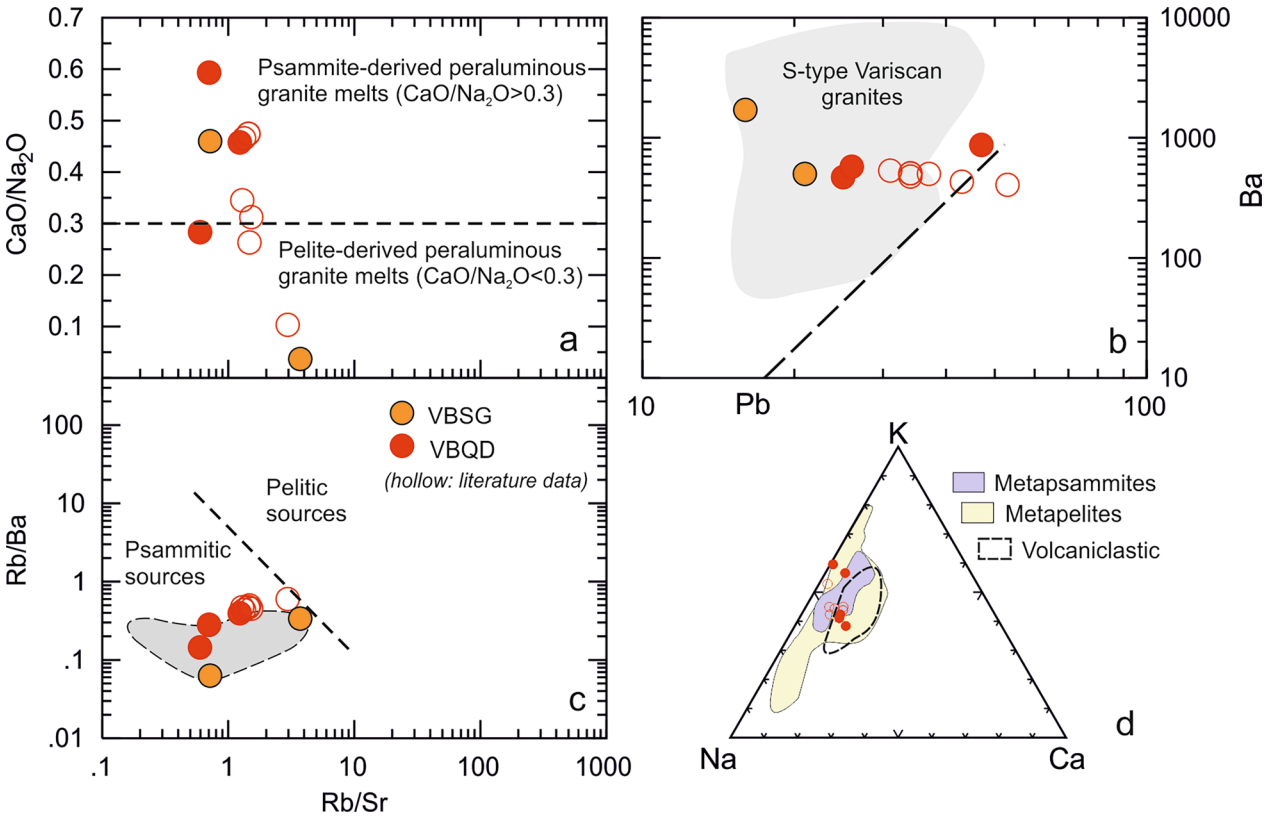

Fig. 17 Composition of the cordierite granites of the VBQD and of granites of the VSBG compared with the compositions of possible rock sources. Most of the rock samples display LILE abundance and ratios (Rb/Ba, Rb/Sr, Ba). Also in terms of major elements (K, and and Ca, **d**), the VBQD and VSBG granites suggest the contribution of partial melting of metapelites and metapsammites during their genesis. Data of the Variscan S-type granites are from Finger & Schiller (2012)

garnet, as also supported by lower Al_2O_3 and Mg# values with respect to the cordierite granite. Therefore, a different magma source could be envisaged for the VSBG granite. We can speculate a low- Mg# metaspammitic source characterized by a more Ca-rich plagioclase and in which less plagioclase undergone melting.

7.3 The Val Biandino Intrusive Suite in the frame of the post-Variscan geodynamic scenario

The Early Permian phase of crustal extension and lithospheric thinning was accompanied by the emplacement of magmatic bodies at different crustal levels and superficial volcanism that lasted ca. 20 Ma, from 295 to 275 Ma (Fig. 13), whit a climax around 280–285 Ma (Schaltegger & Brack, 2007). The extension of the early Permian magmatic belt in Southern Europe could be estimated of ca. 500 km, from Sardinia (Traversa et al., 2003; Renna et al., 2006, 2007; Tribuzio et al., 2009; Boscaini et al., 2020) to the Eastern Alps (Del Moro & Visonà, 1982; Rottura et al., 1998; Marocchi et al., 2008 Boscaini et al., 2020). This belt extended in the southern foreland of the former Variscan orogen, with most of the early Permian magmatic rocks that are now day exposed in the Southalpine, Austroalpine and Penninic domains of the Alps. Despite the short time interval of magmatism duration, significant differences in the geochemical signature occur, mainly expressed in the most basic terms. Gabbros, gabbronorites, troctolites and norites with tholeiitic affinity occur in the Ivrea-Verbano mafic–ultramafic complex (Voshage et al., 1990; Sinigoi et al., 1994; Sinigoi et al., 2016) and in the Central Alps (Braccia-Fedoz gabbro and Sondalo gabbro, Hermann et al., 2001; Tribuzio et al., 1999; Petri et al., 2017), whereas other mafic complexes like whose of the Corsica-Sardinian batholith (Renna et al., 2006, 2007; Tribuzio et al., 2009; Boscaini et al., 2020), the Mt. Collon (Monjoie et al., 2005, 2007) and the minor mafic bodies associated to the Brixen granodiorite (Boscaini et al., 2020) display a subduction-related geochemical signature.

The almost contemporaneous emplacement of these geochemically different mafic magmatic complexes could be interpreted as a response of partial melting processes that affected at different depths an heterogeneous mantle source, composed by depleted or slightly-enriched

regions (e.g. Tribuzio et al., 1999) and enriched ones. The subduction-related metasomatism of the enriched mantle source could be related to the effect of the Variscan subduction. However, the occurrence of subduction-related magmatism could not be taken as an evidence of the presence of a slab beneath the early Permian magmatic belt, as partial melting of the metasomatized mantle could have been triggered in response of asthenospheric upwelling (Bonin et al., 1998) in the frame of the tectonic extensional regime, several Myrs or decades of Mrys after subduction has ceased. The calk-alkaline geochemical signature of the most mafic terms of the Val Biandino Intrusive Suite could thus be explained by partial melting of an already subduction-modified mantle source, likely during the Variscan orogeny, with produced melts that were also later partially contaminated by a crustal component.

In the intermediate and differentiated rock types of the Val Biandino Intrusive Suite, the crustal component becomes predominant. The occurrence of inherited cores within zircon grains of the leucogranites testifies for this process. $^{206}Pb/^{238}U$ ages obtained from zircon inherited cores (Fig. 10 and Table 3) are within the 540–520 Ma and 360–300 Ma time intervals, similar to ages obtained from detrital zircon grains from the Orobic basement (Siegesmund et al., 2023).

This supports the occurrence of crustal anatexis promoted by high heat advection due to asthenosphere upwelling and crystallization of mafic bodies in the lower crust or at the mantle/crust boundary.

8 Conclusions

The Val Biandino Intrusive Suite consists of two distinct units: the Val Biandino Quartz-Diorite (VBQD) and the Valle di San Biagio Granite (VSBG). The VBQD is a heterogeneous magmatic unit, whereas the VBSG consists of a single magmatic body of porphyric granite. Textural features of the VSBG granite suggest shallower depth of intrusion with respect to the VBQD. The two complexes were later juxtaposed by the NW dipping Sassi Rossi Normal Fault (SRNF, Fig. 2) of early to middle Permian age.

SHRIMP U–Pb zircon intrusion ages obtained for the most differentiated terms of the VBQD (285.2 ± 1.9 Ma) and for the VSBG (283.2 ± 1.9 Ma) point to slightly younger ages than previously envisaged. Available data suggest instead that the intermediate terms of the VBQD intruded earlier (289.1 ± 4.5 Ma; Pohl et al., 2018), as also testified by the crosscutting relationships observed in the field.

Despite its relatively small size, the Val Biandino Intrusive Suite displays a marked heterogeneity in terms of rock varieties that intruded in a short time interval (ca. 5 Myrs). Geochemical data suggest that gabbro-diorite, quartz-diorite, granodiorite and leucogranite are not co-magmatic. All the rock types of the Val Biandino Intrusive Suite were likely generated with the significant contribution from melting and/or assimilation of the heterogeneous continental crust forming the pre-Permian Orobic metamorphic basement, with the most mafic terms that preserve evidence of partial melting of a subduction-modified mantle source.

The petrogenetic scenario in which the Val Biandino Intrusive Suite formed could be framed in the early Permian crustal extension than led to heat advection from the asthenosphere. Upper mantle partial melting resulted in the underplating of mafic complex at the lower crust–mantle boundary (e.g. Ivrea-Verbano Zone, Sesia–Lanzo, Valmalenco area) that in turn promoted anatexis also in the lower and middle crust, as the crustal signature occurring in several intermediate to acidic intrusive bodies of early Permian age in several domains of the Alps demonstrates.

Acknowledgements
This work is part of the master's degree thesis of Chiara Crippa. Field and analytical work were funded by the ATE-2015 fund of the university of Milano Bicocca granted to Stefano Zanchetta and Andrea Zanchi. Three anonymous reviewers and editor P. Manzotti provided constructive comments and suggestions that helped to improve the manuscript.

Author contributions
The research project was conceived by SZ and AZ. CC, CM, SZ and AZ performed analyses in the field and labs. SZ and CC were major contributors in writing the manuscript that had been revised by all authors. All authors read and approved the final manuscript.

Funding
Not applicable.

Availability of data and materials
All original data generated and analysed during this study are included in this published article or in supplementary files.

Declarations

Ethics approval and consent to participate
Not applicable.

Consent for publication
Not applicable.

Competing interests
The authors declare that they have no competing interests.

Author details
[1]Dipartimento di Scienze dell'Ambiente e della Terra, Università degli Studi di Milano Bicocca, Piazza della Scienza 4, 20126 Milan, Italy.

Received: 29 September 2023 Accepted: 3 March 2024
Published online: 23 April 2024

References

Aldanmaz, E. R. C. A. N., Pearce, J. A., Thirlwall, M. F., & Mitchell, J. G. (2000). Petrogenetic evolution of late Cenozoic, post-collision volcanism in western Anatolia, Turkey. *Journal of Volcanology and Geothermal Research, 102*(1–2), 67–95.

Altherr, R., Holl, A., Hegner, E., Langer, C., & Kreuzer, H. (2000). High-potassium, calc-alkaline I-type plutonism in the European Variscides: Northern Vosges (France) and northern Schwarzwald (Germany). *Lithos, 50*(1–3), 51–73.

Arth, J. G., & Barker, F. (1976). Rare-earth partitioning between hornblende and dacitic liquid and implications for the genesis of trondhjemitic-tonalitic magmas. *Geology, 4*(9), 534–536.

Arth, J. G., Barker, F., Peterman, Z. E., & Friedman, I. (1978). Geochemistry of the gabbro—diorite—tonalite—trondhjemite suite of southwest Finland and its implications for the origin of tonalitic and trondhjemitic magmas. *Journal of Petrology, 19*(2), 289–316.

Arthaud, F., & Matte, P. (1977). Late Paleozoic strike-slip faulting in southern Europe and northern Africa: Result of a right-lateral shear zone between the Appalachians and the Urals. *Geological Society of America Bulletin, 88*(9), 1305–1320.

Avanzini, M., Bargossi, G. M., Borsato, A. & Selli, L. (2010). *Note illustrative della Carta Geologica d'Italia alla scala 1:50,000, Foglio 060 'Trento'*. ISPRA, Servizio Geologico d'Italia, p. 244.

Bakos, F., Del Moro, A., & Visonà, D. (1990). The Hercynian volcanoplutonic association of Ganna (Lake Lugano, Central Southern Alps, Italy). *European Journal of Mineralogy, 2*, 373–383.

Ballèvre, M., Camonin, A., Manzotti, P., & Poujol, M. (2020). A step towards unraveling the paleogeographic attribution of pre-Mesozoic basement complexes in the Western Alps based on U-Pb geochronology of Permian magmatism. *Swiss Journal of Geosciences, 113*, 1–28.

Barbarin, B. (2005). Mafic magmatic enclaves and mafic rocks associated with some granitoids of the central Sierra Nevada batholith, California: nature, origin, and relations with the hosts. *Lithos, 80*(1–4), 155–177.

Bargossi, G.M., Bove, G., Cucato, M., Gregnanin, A., Morelli, C., Moretti, A., Poli, S., Zanchetta, S., & Zanchi, A. (2010). Note Illustrative della Carta Geologica d'Italia in scala 1:50.000, foglio 013 "Merano". Servizio Geologico d'Italia – ISPRA, p. 316.

Barth, S., Oberli, F., & Meier, M. (1994). Th-Pb versus U-Pb isotope systematics in allanite from co-genetic rhyolite and granodiorite: Implications for geochronology. *Earth and Planetary Science Letters, 124*, 149–159.

Barth, S., Oberli, F., Meier, M., Blattner, P., Bargossi, G. M., & Di Battistini, G. (1993). The evolution of a calc-alkaline basic to silicic magma system: Geochemical and Rb-Sr, Sm-Nd, and $^{18}O^{16}O$ isotopic evidence from the Late Hercynian Atesina-Cima d'Asta volcano-plutonic complex, northern Italy. *Geochimica Et Cosmochimica Acta, 57*(17), 4285–4300.

Beard, J. S., & Lofgren, G. E. (1989). Effect of water on the composition of partial melts of greenstone and amphibolite. *Science, 244*(4901), 195–197.

Beard, J. S., & Lofgren, G. E. (1991). Dehydration melting and water-saturated melting of basaltic and andesitic greenstones and amphibolites at 1, 3, and 6. 9 kb. *Journal of Petrology, 32*(2), 365–401.

Benito, R., López-Ruiz, J., Cebriá, J. M., Hertogen, J., Doblas, M., Oyarzun, R., & Demaiffe, D. (1999). Sr and O isotope constraints on source and crustal contamination in the high-K calc-alkaline and shoshonitic Neogene volcanic rocks of SE Spain. *Lithos, 46*(4), 773–802.

Bergomi, M. A., Dal Piaz, G. V., Malusà, M. G., Monopoli, B., & Tunesi, A. (2017). The Grand St Bernard-Briançonnais nappe system and the Paleozoic inheritance of the Western Alps unraveled by zircon U-Pb dating. *Tectonics, 36*(12), 2950–2972.

Berra, F., & Felletti, F. (2010). Syndepositional tectonics recorded by soft-sediment deformation and liquefaction structures (continental Lower Permian sediments, Southern Alps, Northern Italy): Stratigraphic significance.

Berra, F., Felletti, F., & Tessarollo A. (2016). Stratigraphic architecture of a transtensional continental basin in low-latitude semiarid conditions: The Permian Succession of the Central Orobic Basin (Southern alps, Italy).

Berra, F., & Carminati, E. (2010). Subsidence history from Backstripping analysis of the Permo-Mesozoic succession of the Central Southern Alps (Northern Italy). *Basin Research, 22*, 952–975.

Berra, F., Tiepolo, M., Caironi, V., & Siletto, G. B. (2015). U-Pb zircon geochronology of volcanic deposits from the Permian basin of the Orobic Alps (Southern Alps, Lombardy): Chronostratigraphic and geological implications. *Geological Magazine, 152*, 429–443.

Black, L. P., Kamo, S. L., Allen, C. M., Aleinikoff, J. N., Davis, D. W., Korsch, R. J., & Foudoulis, C. (2003). TEMORA 1: A new zircon standard for Phanerozoic U-Pb geochronology. *Chemical Geology, 200*(1–2), 155–170.

Black, L. P., Kamo, S. L., Allen, C. M., Davis, D. W., Aleinikoff, J. N., Valley, J. W., Mundil, R., Campbell, I. H., Korsch, R. J., Williams, S. W., & Foudoulis, C. (2004). Improved $^{206}Pb/^{238}U$ microprobe geochronology by the monitoring of a trace-element-related matrix effect; SHRIMP, ID–TIMS, ELA–ICP–MS and oxygen isotope documentation for a series of zircon standards. *Chemical Geology, 205*, 115–140.

Blom, J. C., & Passchier, C. W. (1997). Structures along the Orobic thrust, Central Orobic Alps, Italy. *Geologische Rundschau, 86*, 627–636.

Bonin, B. (2004). Do coeval mafic and felsic magmas in post-collisional to within-plate regimes necessarily imply two contrasting, mantle and crustal, sources? A Review. *Lithos, 78*(1–2), 1–24.

Bonin, B., Azzouni-Sekkal, A., Bussy, F., & Ferrag, S. (1998). Alkali-calcic and alkaline post-orogenic (PO) granite magmatism: Petrologic constraints and geodynamic settings. *Lithos, 45*, 45–70.

Boriani, A., Bini, A., & Berra, F. (2012). Note Illustrative della Carta Geologica d'Italia in scala 1:50.000, foglio 056 "Sondrio". Servizio Geologico d'Italia—ISPRA, p. 242.

Boriani, A., Sassi, F., & Sassi, R. (2003). The basement complexes in Italy, with special regards to those exposed in the Alps: A review. *Episodes Journal of International Geoscience, 26*(3), 186–192.

Borsi, S., D'Amico, C., & Del Moro, A. (1974). Studio radiometrico delle rocce intrusive del massiccio di Cima d'Asta (Trentino). *Memorie Della Società Geologica Italiana, 13*, 145–159.

Borsi, S., Ferrara, G., & Tongiorgi, E. (1966). Rb/Sr and K/Ar ages of intrusive rocks of Adamello and M. Sabion (Trentino, Italy). *Earth and Planetary Science Letters, 1*(2), 55–57.

Boscaini, A., Marzoli, A., Davies, J., Chiaradia, M., Bertrand, H., Zanetti, A., Visonà, D., De Min, A., & Jourdan, F. (2020). Permian post-collisional basic magmatism from Corsica to the Southeastern Alps. *Lithos, 376*, 105733.

Brack, P., & Schaltegger, U. (1999). Magmatism and extension in the Lower Permian of the Southern Alps: new age constraints from high-resolution U–Pb dating of zircons. In: International field conference "The Permian of the Southern Alps and Sardinia (Italy)", Brescia, 15–19 September 1999 (Abstr vol).

Breton, N. L., & Thompson, A. B. (1988). Fluid-absent (dehydration) melting of biotite in metapelites in the early stages of crustal anatexis. *Contributions to Mineralogy and Petrology, 99*(2), 226–237.

Broutin, J., Cabanis, B., Chateauneuf, J. J., & Deroin, J. P. (1994). Biostratigraphy, magmatism, and tectonics of the SW European realm during the Permian times with paleogeographic consequences. *Bulletin De La Société Géologique De France, 165*, 163–179.

Burg, J. P., van der Driessche, J., & Brun, J. P. (1994). L'extension syn-a-post-épaississement de la chaîne varisque en Europe occidentale : Modalités et conséquences. *Colloque Géologie De La France, 3*, 33–51.

Cadel, G., Cosi, M., Pennacchioni, G., & Spalla, M. I. (1996). A new map of the Permo-Carboniferous cover and Variscan metamorphic basement in the Central Orobic Alps, Southern Alps-Italy: Structural and stratigraphical data. *Memorie Di Scienze Geologiche Padova, 48*, 1–53.

Cagnard, F., Gapais, D., Brun, J. P., Gumiaux, C., & Van der Driessche, J. (2004). Late pervasive crustal-scale extension in the south Armorican Hercynian belt (Vendée, France). *Journal of Structural Geology, 26*, 435–449.

Capuzzo, N., & Wetzel, A. (2004). Facies and basin architecture of the Late Carboniferous Salvan-Dorénaz continental basin (Western Alps, Switzerland/France). *Sedimentology, 51*(4), 675–697.

Carlson, R. W. (1991). Physical and chemical evidence on the cause and source characteristics of flood basalt volcanism. *Australian Journal of Earth Sciences, 38*(5), 525–544.

Carminati, E., Siletto, G. B., & Battaglia, D. (1997). Thrust kinematics and internal deformation in basement-involved fold and thrust belts: The eastern Orobic Alps case (Central Southern Alps, northern Italy). *Tectonics, 16*(2), 259–271.

Casati, P., & Gnaccolini, M. (1967). Geologia delle Alpi Orobie occidentali. *Rivista Italiana d Paleontologia e Stratigrafia, 73*, 25–162.

Casini, L., & Oggiano, G. (2008). Late orogenic collapse and thermal doming in the northern Gondwana margin incorporated in the Variscan Chain: A

case study from the Ozieri Metamorphic Complex, northern Sardinia, Italy. *Gondwana Research, 13*(3), 396–406.
Cassinis, G., Cortesogno, L., Gaggero, L., Perotti, C., & Ronchi, A. (2007). Volcanic products from the Early Permian Collio Basin (southern Alps) and their geodynamic implications. *Periodico Di Mineralogia, 76*, 25–47. https://doi.org/10.2451/2007PM0007
Cassinis, G., Massari, F., Neri, C., & Venturini, C. (1988). The continental Permian in the Southern Alps. *Zeitschrift Für Geologische Wissenschaften, 16*, 1117–1126.
Cassinis, G., & Perotti, C. R. (1994). Interazione strutturale permiana tra la linea delle Giudicarie ed i bacini di Collio, Tione e Tragiovo (Sudalpino centrale, N. Italia). *Bollettino della Società Geologica Italiana*, *112*(3–4), 1021–1036.
Cassinis, G., Perotti, C. R., & Ronchi, A. (2012). Permian continental basins in the Southern Alps (Italy) and peri-mediterranean correlations. *International Journal of Earth Science, 101*, 129–157.
Castro, A., & Stephens, W. E. (1992). Amphibole-rich polycrystalline clots in calc-alkaline granitic rocks and their enclaves. *The Canadian Mineralogist, 30*(4), 1093–1112.
Chappell, B. W., & White, A. J. (2001). Two contrasting granite types: 25 years later. *Australian Journal of Earth Sciences, 48*(4), 489–499.
Clarke, D. B. (1995). Cordierite in felsic igneous rocks: A synthesis. *Mineralogical Magazine, 59*(395), 311–325.
Clemens, J. D., & Vielzeuf, D. (1987). Constraints on melting and magma production in the crust. *Earth and Planetary Science Letters, 86*(2–4), 287–306.
Clemens, J. D., & Wall, V. J. (1981). Origin and crystallization of some peraluminous (S-type) granitic magmas. *The Canadian Mineralogist, 19*(1), 111–131.
Condie, K. C. (1993). Chemical composition and evolution of the upper continental crust: Contrasting results from surface samples and shales. *Chemical Geology, 104*(1–4), 1–37.
Corfu, F., Hanchar, J. M., Hoskin, P. W., & Kinny, P. (2003). Atlas of zircon textures. *Reviews in Mineralogy and Geochemistry, 53*(1), 469–500.
Cornelius, H. P. (1916). Zur Kenntnis der Wurzelregion im unteren Veltlin. *N Jahr Min Geol Paläont, 40*, 253–363.
Cortesogno, L., Cassinis, G., Dallagiovanna, G., Gaggero, L., Oggiano, G., Ronchi, A., Seno, S., & Vanossi, M. (1998). The Variscan post-collisional volcanism in late Carboniferous-Permian sequences of Ligurian Alps, southern Alps and Sardinia (Italy): A synthesis. *Lithos, 45*(1–4), 305–328.
Crommelin, R. (1932). La géologie de la Valsassina et de la region adiacente au Nord. Crommelin, R. D. (1931). La Géologie de la Valsassina et de la région adjacente au Nord. *Leiden Geologische Mededelingen*, *4*(1), 403–459.
Cumming, G. L., & Richards, J. R. (1975). Ore lead isotope ratios in a continuously changing Earth. *Earth and Planetary Science Letters, 28*(2), 155–171.
D'Adda, P., & Zanchetta, S. (2015). Geological-structural map of the Orobic and Porcile thrust junction, central southern Alps (N Italy). *Journal of Maps, 11*(1), 25–38.
De Capitani, L. (1982). Contributo alla conoscenza dei plutoni sudalpini: Le masse intrusive della Val Biandino (Como). *Rendiconti Della Società Italiana Di Mineralogia e Petrografia, 38*, 109–118.
De Capitani, L., Delitala, M. C., Liborio, G., Mottana, A., Nicoletti, M., & Petrucciani, C. (1988). K-Ar dating of the Val Biandino Plutonic complex. *Memorie Di Scienze Geologiche Padova, XL*, 285–294.
De Capitani, L., Delitalia, M. C., Liborio, G., Mottana, A., Rodeghiero, F., & Thöni, M. (1994). The granitoid rocks of Val Navazze, Val Torgola and Val di Rango (Val Trompia, Lombardy, Italy). *Memorie Di Scienze Geologiche (padova), 46*, 329–343.
De Capitani, L., & Liborio, G. (1988). Trace element abundance in the Val Biandino pluton (Southern Alps, Italy). *Memorie Di Scienze Geologiche Padova, 40*, 99–100.
De Capitani, L., Moroni, M., & Rodeghiero, F. (1999). Geological and geochemical characteristics of Permian tourmalinitization at Val Trompia (southern Alps, northern Italy) and relationship with the Orobic tourmalinites.
De Sitter, L. U., & De Sitter-Koomans, C. M. (1949). Geology of the Bergamasc Alps, Lombardia, Italy. *Leiden Geologische Mededelingen, 14*, 1–257.
Del Moro, A., & Visonà, D. (1982). The epiplutonic Hercynian complex of Bressanone (Brixen, eastern Alps, Italy), Petrologic and radiometric data. *Neues Jahrbuch Für Mineralogie. Abhandlungen, 145*, 66–85.
Dewey, J. F. (1988). Extensional collapse of orogens. *Tectonics, 7*(6), 1123–1139.
Diella, V., Spalla, M. I., & Tunesi, A. (1992). Contrasting thermomechanical evolutions in the Southalpine metamorphic basement of the Orobic Alps (Central Alps, Italy). *Journal of Metamorphic Geology, 10*, 203–219.
Downes, H., Kostoula, T., Jones, A., Beard, A., Thirlwall, M., & Bodinier, J. L. (2002). Geochemistry and Sr–Nd isotopic compositions of mantle xenoliths from the Monte Vulture carbonatite–melilitite volcano, central southern Italy. *Contributions to Mineralogy and Petrology, 144*(1), 78–92.
Echtler, H., & Malavieille, J. (1990). Extensional tectonics, basement uplift and Stephano-Permian collapse basin in a late Variscan metamorphic core complex (Montagne Noire, Southern Massif Central). *Tectonophysics, 177*(1–3), 125–138.
Finger, F., & Schiller, D. (2012). Lead contents of S-type granites and their petrogenetic significance. *Contributions to Mineralogy and Petrology, 164*(5), 747–755.
Fréville, K., Trap, P., Vanardois, J., Melleton, J., Faure, M., Bruguier, O., Poujol, M., & Lach, P. (2022). Carboniferous-Permian tectono-metamorphic evolution of the Pelvoux Massif (External Crystalline Massif, Western Alps), with discussion on flow kinematics of the Eastern-Variscan Shear Zone. *Bulletin De La Société Géologique De France*. https://doi.org/10.1051/bsgf/2022008
Froitzheim, N., Derks, J. F., Walter, J. M., & Sciunnach, D. (2008). Evolution of an Early Permian extensional detachment fault from synintrusive, mylonitic flow to brittle faulting (Grassi Detachment Fault, Orobic Anticline, southern Alps, Italy). *Geological Society of London, Special Publication, 298*, 69–82.
Gaetani, M., Gianotti, R., Jadoul, F., Ciarapica, G., Cirilli, S., Lualdi, A., Passeri, L., Pellegrini, M., & Tannoia, G. (1986). Carbonifero Superiore, Permiano e Triassico nell'area Lariana. *Memorie Della Società Geologica Italiana, 32*, 5–48.
Gaetani, M., Sciunnach, D., Bini, A., & Rossi, S. (2012). Note illustrative della Carta Geologica d'Italia alla scala 1:50.000, F. 076 Lecco. ISPRA, Servizio Geologico d'Italia, Roma.
Garuti, G., Bea, F., Zaccarini, F., & Montero, P. (2001). Age, geochemistry and petrogenesis of the ultramafic pipes in the Ivrea Zone, NW Italy. *Journal of Petrology, 42*, 433–457.
Gill, J. B. (1981). What is "Typical Calcalkaline Andesite"? In J. B. Gill (Ed.), *Orogenic Andesites and Plate Tectonics* (pp. 1–12). Springer Berlin Heidelberg. https://doi.org/10.1007/978-3-642-68012-0_1
Gretter, N., Ronchi, A., Langone, A., & Perotti, C. R. (2013). The transition between the two major Permian tectono-stratigraphic cycles in the central Southern Alps: Results from facies analysis and U/Pb geochronology. *International Journal of Earth Sciences, 102*(5), 1181–1202.
Harris, N., Ayres, M., & Massey, J. (1995). Geochemistry of granitic melts produced during the incongruent melting of muscovite: Implications for the extraction of Himalayan leucogranite magmas. *Journal of Geophysical Research: Solid Earth, 100*(B8), 15767–15777.
Harris, N. B. W., & Inger, S. (1992). Trace element modelling of pelite-derived granites. *Contributions to Mineralogy and Petrology, 110*(1), 46–56.
Hartmann, G., & Wedepohl, K. H. (1993). The composition of peridotite tectonites from the Ivrea complex (N-Italy) Residues from melt extraction. *Geochimica Cosmochima Acta, 57*, 1761–1782.
Hawkesworth, C. J. (1980). $^{143}Nd/^{144}Nd$, $^{87}Sr/^{86}Sr$ and trace element characteristics of magmas along destructive plate margins. In M. P. Atherton & J. Tarney (Eds.), *Origin of granite batholiths* (pp. 76–89). Birkhäuser Boston. https://doi.org/10.1007/978-1-4684-0570-5_7
Hawkesworth, C. J., Marsh, J. S., Duncan, A. R., Erlank, A. J., & Norry, M. J. (1984). *The role of continental lithosphere in the generation of the Karoo volcanic rocks: Evidence from combined Nd-and Sr-isotope studies*. Special Publication.
Hawkesworth, C., Turner, S., Gallagher, K., Hunter, A., Bradshaw, T., & Rogers, N. (1995). Calc-alkaline magmatism, lithospheric thinning and extension in the Basin and Range. *Journal of Geophysical Research: Solid Earth, 100*(B6), 10271–10286.
Hawkesworth, C. J., & Vollmer, R. (1979). Crustal contamination versus enriched mantle: $^{143}Nd/1^{44}Nd$ and $^{87}Sr/^{86}Sr$ evidence from the Italian volcanics. *Contributions to Mineralogy and Petrology, 69*(2), 151–165.
Hergt, J. M., Peate, D. W., & Hawkesworth, C. J. (1991). The petrogenesis of Mesozoic Gondwana low-Ti flood basalts. *Earth and Planetary Science Letters, 105*(1–3), 134–148.

Hermann, J., Muntener, O., & Gunther, D. (2001). Differentiation of mafic magma in a continental crust-to-mantle transition zone. *Journal of Petrology, 42*, 189–206.
Hildreth, W., & Moorbath, S. (1988). Crustal contributions to arc magmatism in the Andes of central Chile. *Contributions to Mineralogy and Petrology, 98*(4), 455–489.
Holtz, F., & Johannes, W. (1991). Genesis of peraluminous granites I. Experimental investigation of melt compositions at 3 and 5 kb and various H2O activities. *Journal of Petrology, 32*(5), 935–958.
Hooper, P. R., & Hawkesworth, C. J. (1993). Isotopic and geochemical constraints on the origin and evolution of the Columbia River Basalt. *Journal of Petrology, 34*(6), 1203–1246.
Inger, S., & Harris, N. (1993). Geochemical constraints on leucogranite magmatism in the Langtang Valley, Nepal Himalaya. *Journal of Petrology, 34*(2), 345–368.
Kilian, R., & Stern, C. R. (2002). Constraints on the interaction between slab melts and the mantle wedge from adakitic glass in peridotite xenoliths. *European Journal of Mineralogy, 14*(1), 25–36.
Klötzli, U. S., Mair, V., & Bargossi, G. M. (2003). The "Bozener Quarzporphyr"(Southern Alps, Italy): Single zircon U/Pb age evidence for 10 million years of magmatic activity in the Lower Permian. *Mitteilungen Der Österreichischen Mineralogischen Gesellschaft, 148*, 187–188.
Klötzli, U. S., Sinigoi, S., Quick, J. E., Demarchi, G., Tassinari, C. C., Sato, K., & Günes, Z. (2014). Duration of igneous activity in the Sesia Magmatic System and implications for high-temperature metamorphism in the Ivrea-Verbano deep crust. *Lithos, 206*, 19–33.
Lardeaux, J. M., & Spalla, M. I. (1991). From granulites to eclogites in the Sesia zone (Italian Western Alps): A record of the opening and closure of the Piedmont ocean. *Journal of Metamorphic Geology, 9*(1), 35–59.
Laubscher, H. P. (1985). Large-scale, thin-skinned thrusting in the southern Alps: Kinematic models. *Geological Society of America Bulletin, 96*, 710–718.
Le Pichon, X., Jellinek, M., Lenardic, A., Sengör, A. M., & Imren, C. (2021). Pangea Migration. *Tectonics*. https://doi.org/10.1029/2020TC006585
Le Pichon, X., Sengör, A. M., & Imren, C. (2019). Pangea and the Lower Mantle. *Tectonics*. https://doi.org/10.1029/2018TC005445
Locchi, S. (2023). The post-Variscan evolution of the central Southern Alps: Insights from synchronous fault activity, hydrothermalism and magmatism in the Orobic and Collio basins. PhD Thesis, University of Milano Bicocca, p. 187.
Locchi, S., Zanchetta, S., & Zanchi, A. (2022). Evidence of Early Permian extension during the post-Variscan evolution of the central Southern Alps (N Italy). *International Journal of Earth Sciences, 111*(6), 1717–1738.
Macera, P., Del Moro, A., Bargossi, G. M., Campana, R., & Rottura, A. (1994). Polygenetic nature of the Cima d'Asta intrusive complex, Southern Alps, Italy. Inferences from petrological, geochemical and isotopic (Sr and Nd) data. *Lithos, 32*, 47–62.
Mahoney, J. J. (1988). Deccan traps. In J. D. Macdougall (Ed.), *Continental flood basalts* (pp. 151–194). Springer Dordrecht. https://doi.org/10.1007/978-94-015-7805-9_5
Malavieille, J. (1993). Late orogenic extension in mountain belts: Insights from the Basin and Range and the late Paleozoic Variscan belt. *Tectonics, 12*(5), 1115–1130.
Malavieille, J., Guihot, P., Costa, S., Lardeaux, J. M., & Gardien, V. (1990). Collapse of the thickened Variscan crust in the French Massif Central: Mont Pilat extensional shear zone and St. Etienne Late Carboniferous Basin. *Tectonophysics, 177*(1–3), 139–149.
Manzotti, P., Poujol, M., & Ballèvre, M. (2015). Detrital zircon geochronology in blueschist-facies meta-conglomerates from the Western Alps: Implications for the late Carboniferous to early Permian paleogeography. *International Journal of Earth Sciences, 104*, 703–731.
Marocchi, M., Morelli, C., Mair, V., Klötzli, U., & Bargossi, G. M. (2008). Evolution of large silicic magma systems: New U-Pb zircon data on the NW Permian Athesian Volcanic Group (Southern Alps, Italy). *The Journal of Geology, 116*(5), 480–498.
McCann, T., Pascal, C., Timmerman, M. J., Krzywiec, P., López-Gómez, J., Wetzel, L., Krawczyk, C. M., Rieke, H., & Lamarche, J. (2006). Post-Variscan (end Carboniferous-Early Permian) basin evolution in western and central Europe. *Geological Society, London, Memoirs, 32*(1), 355–388.
McDonough, W. F., & Sun, S. S. (1995). The composition of the Earth. *Chemical Geology, 120*(3–4), 223–253.
Ménard, G., & Molnar, P. (1988). Collapse of a Hercynian Tibetan plateau into a late Palaeozoic European Basin and Range province. *Nature, 334*(6179), 235–237.
Menzies, M. A., Rogers, N., Tindle, A., & Hawkesworth, C. J. (1987). Metasomatic and enrichment processes in lithospheric peridotites, an effect of asthenosphere-lithosphere interaction. Mantle metasomatism (pp. 313–361). Academic Press, London.
Milano, P. F., Pennacchioni, G., & Spalla, M. I. (1988). Alpine and pre-Alpine tectonics in the central Orobic Alps (Southern Alps). *Eclogae Geologicae Helvetiae, 81*, 273–293.
Miller, C. F. (1985). Are strongly peraluminous magmas derived from pelitic sedimentary sources? *The Journal of Geology, 93*(6), 673–689.
Mittempergher, S., Zanchi, A., Zanchetta, S., Fumagalli, M., Gukov, K., & Bistacchi, A. (2021). Fault reactivation and propagation in the northern Adamello pluton: The structure and kinematics of a kilometre-scale seismogenic source. *Tectonophysics, 806*, 228790.
Monjoie, P., Bussy, F., Lapierre, H., & Pfeifer, H. R. (2005). modelling of in-situ crystallizationprocesses in themfic layered intrusion of Mont Collon (Dent Blanche nappe, western Alps). *Lithos, 83*, 317–346.
Monjoie, P., Bussy, F., Schaltegger, U., Mulch, A., Lapierre, H., & Pfeifer, H. R. (2007). Contrasting magma types and time of intrusion in the Permian layered mafic complex of Mont Collon(Western Alps, Valais, Switzerland): Evidence from U/Pb zircon and $^{40}Ar/^{39}Ar$ amphibole dating. *Swiss Journal of Geosciences, 100*, 125–135.
Montel, J. M., Weber, C., & Pichavant, M. (1986). Biotite-sillimanite-spinel assemblages in high-grade metamorphic rocks: Occurrences, chemographic analysis and thermobarometric interest. *Bulletin of Mineralogy, 109*, 555–557.
Morelli, C., Marocchi, M., Moretti, A., Bargossi, G. M., Gasparotto, G., De Waele, B., Klötzli, U., & Mair, V. (2012). Volcanic stratigraphy and radiometric age constraints at the northern margin of a mega-caldera system: Athesian Volcanic Group (Southern Alps, Italy). *GeoActa, 11*, 51–67.
Müntener, O., Hermann, J., & Trommsdorff, V. (2000). Cooling history and exhumation of lower-crustal granulite and upper mantle (Malenco, Eastern Central Alps). *Journal of Petrology, 41*(2), 175–200.
Muttoni, G., Kent, D. V., Garzanti, E., Brack, P., Abrahamsen, N., & Gaetani, M. (2003). Early Permian Pangea 'B' to Late Permian Pangea 'A.' *Earth and Planetary Science Letters, 215*(3–4), 379–394.
Obermiller, W. A. (1994). Chemical and isotopic variations in the Balmuccia, Baldissero and Finero peridotite massifs (Ivrea-Zone, N-Italy) (PhD Thesis, Verlag nicht ermittelbar).
O'Brien, H. E., Irving, A. J., McCallum, I. S., & Thirlwall, M. F. (1995). Strontium, neodymium, and lead isotopic evidence for the interaction of post-subduction asthenospheric potassic mafic magmas of the Highwood Mountains, Montana, USA, with ancient Wyoming craton lithospheric mantle. *Geochimica Et Cosmochimica Acta, 59*(21), 4539–4556.
Pasquarè, G. (1967). Analisi geologico-strutturale del complesso intrusivo di Val Biandino (Alpi Orobie Occidentali). *Memorie Della Società Geologica Italiana, 6*, 343–357.
Patiño Douce, A. E., & Harris, N. (1998). Experimental constraints on Himalayan anatexis. *Journal of Petrology, 39*(4), 689–710.
Peressini, G., Quick, J. E., Sinigoi, S., Hofmann, A. W., & Fanning, M. (2007). Duration of a large mafic intrusion and heat transfer in the lower crust: A SHRIMP U-Pb zircon study in the Ivrea-Verbano Zone (Western Alps, Italy). *Journal of Petrology, 48*(6), 1185–1218.
Perfit, M. R., Gust, D. A., Bence, A. E., Arculus, R. J., & Taylor, S. R. (1980). Chemical characteristics of island-arc basalts: Implications for mantle sources. *Chemical Geology, 30*(3), 227–256.
Petri, B., Mohn, G., Skrzypek, E., Mateeva, T., Galster, F., & Manatschal, G. (2017). U-Pb geochronology of the Sondalo gabbroic complex (Central Alps) and its position within the Permian post-Variscan extension. *International Journal of Earth Sciences, 106*(8), 2873–2893.
Piccin, G., Morelli, C., Bargossi, G.M., Mair, V., Marocchi, M., & Moretti, A. (2009). Evolution of a magmatic continental megasystem in the Lower Permian. https://doi.org/10.1474/Epitome.03.1195. Geoitalia 2009, p. 322.
Pin, C. (1986). Datation U-Pb sur zircons à 285 Ma du complexe gabbro–dioritique du Val Sesia-Val Mastallone et aˆ ge tardihercynien du métamorphisme granulitique de la zone Ivrea-Verbano (Italie). *Comptes Rendus De L'académie Des Sciences, 303*(9), 827–830.

Pinarelli, L., & Boriani, A. (2007). Tracing metamorphism, magmatism and tectonics in the southern Alps (Italy): Constraints from Rb-Sr and Pb-Pb geochronology, and isotope geochemistry. *Periodico Di Mineralogia, 76*, 5–24.

Pinarelli, L., Del Moro, A., & Boriani, A. (1988). Rb-Sr geochronology of Lower Permian plutonism in Massiccio dei Laghi, Southern Alps (NW Italy). *Rendiconti Della Società Italiana Di Mineralogia e Petrografia, 43*, 411–428.

Pinarelli, L., Moro, A. D., Boriani, A., & Caironi, V. (2002). Sr, Nd isotope evidence for an enriched mantle component in the origins of the Hercynian gabbro-granite series of the "Serie dei Laghi"(Southern Alps, NW Italy). *European Journal of Mineralogy, 14*(2), 403–415.

Plank, T., & Langmuir, C. H. (1993). Tracing trace elements from sediment input to volcanic output at subduction zones. *Nature, 362*(6422), 739–743.

Pohl, F., Froitzheim, N., Obermüller, G., Tomaschek, F., Schröder, O., Nagel, T. J., Sciunnach, D., & Heuser, A. (2018). Kinematics and age of syn-intrusive detachment faulting in the Southern Alps: Evidence for Early Permian crustal extension and implications for the Pangea A versus B Controversy. *Tectonics, 37*(10), 3668–3689.

Porro, C. (1897). Cenni preliminari ad un rilievo geologico nelle Alpi Orobie (Valsassina e Pizzo dei Tre Signori). *Rendiconti Reale Istituto Lombardo Di Scienze e Lettere, 30*, 1–15.

Quick, J. E., Sinigoi, S., Peressini, G., Demarchi, G., Wooden, J. L., & Sbisà, A. (2009). Magmatic plumbing of a large Permian caldera exposed to a depth of 25 km. *Geology, 37*(7), 603–606.

Quick, J. E., Sinigoi, S., Snoke, A. W., Kalakay, T. J., Mayer, A., & Peressini, G., (2003). Geologic map of the Southern Ivrea-Verbano Zone, Northwestern Italy. U.S. Geological Survey, Reston, Virgina, VA.

Rapp, R. P., Shimizu, N., Norman, M. D., & Applegate, G. S. (1999). Reaction between slab-derived melts and peridotite in the mantle wedge: experimental constraints at 3.8 GPa. *Chemical Geology, 160*(4), 335–356.

Rapp, R. P., & Watson, E. B. (1995). Dehydration melting of metabasalt at 8–32 kbar: Implications for continental growth and crust-mantle recycling. *Journal of Petrology, 36*(4), 891–931.

Rapp, R. P., Watson, E. B., & Miller, C. F. (1991). Partial melting of amphibolite/eclogite and the origin of Archean trondhjemites and tonalites. *Precambrian Research, 51*(1–4), 1–25.

Rebay, G., & Spalla, M. I. (2001). Emplacement at granulite facies conditions of the Sesia-Lanzo metagabbros: An early record of Permian rifting? *Lithos, 58*(3–4), 85–104.

Renna, M. R., Tribuzio, R., & Tiepolo, M. (2006). Interaction between basic and acid magmas during the latest stages of the post-collisional Variscan evolution: Clues from the gabbro-granite association of Ota (Corsica-Sardinia batholith). *Lithos, 90*, 92–110.

Renna, M. R., Tribuzio, R., & Tiepolo, M. (2007). Origin and timing of the post-Variscan gabbrogranite complex of Porto (Western Corsica). *Contributions to Mineralogy and Petrology, 154*, 493–517.

Rivalenti, G. (1975). The origin of the Ivrea-Verbano basic formation (Western Italian Alps)—Whole rock geochemistry. *Bollettino Della Società Geologica Italiana, 94*, 1149–1186.

Roberts, M. P., & Clemens, J. D. (1993). Origin of high-potassium, calc-alkaline I-Type Granitoids. *Geology, 21*(9), 825–828.

Rottura, A., Bargossi, G. M., Caggianelli, A., Del Moro, A., Visona, D., & Tranne, C. A. (1998). Origin and significance of the Permian high-K calc-alkaline magmatism in the central-eastern Southern Alps, Italy. *Lithos, 45*(1–4), 329–348.

Rushmer, T. (1991). Partial melting of two amphibolites: Contrasting experimental results under fluid-absent conditions. *Contributions to Mineralogy and Petrology, 107*(1), 41–59.

Rutter, M. J., & Wyllie, P. J. (1988). Melting of vapour-absent tonalite at 10 kbar to simulate dehydration–melting in the deep crust. *Nature, 331*(6152), 159–160.

Saunders, A. D., Tarney, J., & Weaver, S. D. (1980). Transverse geochemical variations across the Antarctic Peninsula: Implications for the genesis of calc-alkaline magmas. *Earth and Planetary Science Letters, 46*(3), 344–360.

Schaltegger, U., & Brack, P. (1999). Short-lived events of extension and volcanism in the Lower Permian of the Southern Alps (Northern Italy, Southern Switzerland). *Journal of Conference Abstracts, 4*, 296–297.

Schaltegger, U., & Brack, P. (2007). Crustal-scale magmatic systems during intracontinental strike-slip tectonics: U, Pb and Hf isotopic constraints from Permian magmatic rocks of the Southern Alps. *International Journal of Earth Sciences, 96*, 1131–1151.

Schmid, S.M., Aebli, H.R., Heller, F., & Zingg, A. (1989). The role of the Periadriatic Line in the tectonic evolution of the Alps. In: Coward, M.P., Dietrich, D., Park, R.G. (Eds.), Alpine Tectonics. *Special Publication Geological Society of London, 45*, 153–171.

Schönborn, G. (1992). Alpine tectonics and kinematic models of the Central Southern Alps. *Memorie Di Scienze Geologiche Padova, 44*, 229–393.

Sciunnach, D. (2001a). The Lower Permian in the Orobic Anticline (Southern Alps, Lombardy): A review based on new stratigraphic and petrographic data. *Rivista Italian Di Paleontologia e Stratigrafia, 107*, 47–68.

Sciunnach, D. (2001b). Early Permian palaeofaults at the western boundary of the Collio Basin (Valsassina, Lombardy). *Natura Bresciana, 25*, 37–43.

Sciunnach, D. (2003). Fault-controlled stratigraphic architecture and magmatism in the Western Orobic Basin (Lower Permian, Lombardy Southern Alps). *Bollettino Della Società Geologica Italiana, 2*, 49–58.

Sedimentary Geology, 235 (3–4), 249–263

Sengupta, S., Bandyopadhyay, P. K., & Van den Hul, H. J. (1983). Geochemistry of the Chakradharpur granite—Gneiss complex—A Precambrian trondhjemite body from West Singhbhum Eastern India. *Precambrian Research, 23*(1), 57–78.

Sial, A. N., Ferreira, V. P., Fallick, A. E., & Cruz, M. J. M. (1998). Amphibole-rich clots in calc-alkalic granitoids in the Borborema province, northeastern Brazil. *Journal of South American Earth Sciences, 11*(5), 457–471.

Siegesmund, S., Oriolo, S., Broge, A., Hueck, M., Lammerer, B., Basei, M., & Schulz, B. (2023). Cadomian to Cenerian accretionary orogenic processes in the Alpine basement: The detrital zircon archive. *International Journal of Earth Sciences, 112*, 1157–1174.

Siletto, G. B., Spalla, M. I., Tunesi, A., Lardeaux, J. M., & Colombo, A. (1993). Pre-Alpine structural and metamorphic histories in the Orobic Southern Alps, Italy. In J. F. von Raumer & F. Neubauer (Eds.), *Pre-Mesozoic geology of the Alps* (pp. 585–598). Springer.

Sinigoi, S., Antonini, P., Demarchi, G., Longinelli, A., Mazzucchelli, M., Negrini, L., & Rivalenti, G. (1991). Interactions of mantle and crustal magmas in the southern part of the Ivrea Zone (Italy). *Contributions to Mineralogy and Petrology, 108*, 385–395.

Sinigoi, S., Quick, J. E., Clemens-Knott, D., Mayer, A., Demarchi, G., Mazzucchelli, M., Negrini, L., & Rivalenti, G. (1994). Chemical evolution of a large mafic intrusion in the lower crust, Ivrea-Verbano Zone, northern Italy. *Journal of Geophysical Research, 99*, 21575–21590.

Sinigoi, S., Quick, J. E., Demarchi, G., & Klötzli, U. (2011). The role of crustal fertility in the generation of large silicic magmatic systems triggered by intrusion of mantle magma in the deep crust. *Contributions to Mineralogy and Petrology, 162*(4), 691–707.

Sinigoi, S., Quick, J. E., Demarchi, G., & Klötzli, U. (2016). Production of hybrid magma at the advancing front of basaltic underplating: Inferecences from the Sesia Magmatic System (south-western Alps, Italy). *Lithos, 252–253*, 109–122.

Sisson, T. W., Ratajeski, K., Hankins, W. B., & Glazner, A. F. (2005). Voluminous granitic magmas from common basaltic sources. *Contributions to Mineralogy and Petrology, 148*(6), 635–661.

Skjerlie, K. P., & Douce, A. E. (1995). Anatexis of interlayered amphibolite and pelite at 10 kbar: Effect of diffusion of major components on phase relations and melt fraction. *Contributions to Mineralogy and Petrology, 122*(1), 62–78.

Skjerlie, K. P., & Johnston, A. D. (1992). Vapor-absent melting at 10 kbar of a biotite-and amphibole-bearing tonalitic gneiss: Implications for the generation of A-type granites. *Geology, 20*(3), 263–266.

Skjerlie, K. P., & Johnston, A. D. (1996). Vapour-absent melting from 10 to 20 kbar of crustal rocks that contain multiple hydrous phases: Implications for anatexis in the deep to very deep continental crust and active continental margins. *Journal of Petrology, 37*(3), 661–691.

Soesoo, A. (2000). Fractional crystallization of mantle-derived melts as a mechanism for some I-type granite petrogenesis: An example from Lachlan Fold Belt, Australia. *Journal of the Geological Society, 157*(1), 135–149.

Spalla, M. I., Carminati, E., Ceriani, S., Oliva, A., & Battaglia, D. (1999). Influence of deformation partitioning and metamorphic re-equilibration on P-T path reconstruction in the pre-Alpine basement of central southern Alps (northern Italy). *Journal of Metamorphic Geology, 17*, 319–336.

Spalla, M. I., Zanoni, D., Marotta, A. M., Rebay, G., Roda, M., Zucali, M., & Gosso, G. (2014). The transition from Variscan collision to continental break-up in the Alps: insights from the comparison between natural data and

numerical model predictions. *Geological Society, London, Special Publications, 405*(1), 363–400.
Steck, A., Della Torre, F., Keller, F., Pfeifer, H. R., Hunziker, J., & Masson, H. (2013). Tectonics of the Lepontine Alps: Ductile thrusting and folding in the deepest tectonic levels of the Central Alps. *Swiss Journal of Geosciences, 106*(3), 427–450.
Stein, M., Navon, O., & Kessel, R. (1997). Chromatographic metasomatism of the Arabian—Nubian lithosphere. *Earth and Planetary Science Letters, 152*(1–4), 75–91.
Stephens, W. E. (2001). Polycrystalline amphibole aggregates (clots) in granites as potential I-type restite: An ion microprobe study of rare-earth distributions. *Australian Journal of Earth Sciences, 48*(4), 591–601.
Stern, R. J. (2002). Subduction Zones. *Reviews of Geophysics, 40*(4), 3–1.
Stevens, G., Clemens, J. D., & Droop, G. T. (1997). Melt production during granulite-facies anatexis: Experimental data from "primitive" metasedimentary protoliths. *Contributions to Mineralogy and Petrology, 128*(4), 352–370.
Sun, C. H., & Stern, R. J. (2001). Genesis of Mariana shoshonites: Contribution of the subduction component. *Journal of Geophysical Research: Solid Earth, 106*(B1), 589–608.
Sylvester, P. J. (1998). Post-collisional strongly peraluminous granites. *Lithos, 45*(1–4), 29–44.
Thirlwall, M. F., & Graham, A. M. (1984). Evolution of high-Ca, high-Sr C-series basalts from Grenada, Lesser Antilles: The effects of intra-crustal contamination. *Journal of the Geological Society, 141*(3), 427–445.
Thirlwall, M. F., Graham, A. M., Arculus, R. J., Harmon, R. S., & Macpherson, C. G. (1996). Resolution of the effects of crustal assimilation, sediment subduction, and fluid transport in island arc magmas: PbSrNdO isotope geochemistry of Grenada Lesser Antilles. *Geochimica Et Cosmochimica Acta, 60*(23), 4785–4810.
Thompson, A. B. (2001). Clockwise P-T paths for crustal melting and H2O recycling in granite source regions and migmatite terrains. *Lithos, 56*(1), 33–45.
Thöni, M., Mottana, A., Delitala, M., De Capitani, L., & Liborio, G. (1992). The Val Biandino composite pluton: A late Hercynian intrusion into the South-Alpine metamorphic basement of the Alps (Italy). *Neues Jahrbuch Für Mineralogie Monatshefte, 12*, 545–554.
Tompson, A. B. (1982). Dehydration melting of pelitic rocks and the generation of H_2O-undersaturated granitic liquids. *American Journal of Sciences, 282*, 1567–1595.
Traversa, G., Ronca, S. S., Del Moro, A., Pasquali, C., Buraglini, N., & Barabino, G. (2003). Late to post-Hercynian dyke activity in the Sardinia-Corsica Domain: a transition from orogenic calc-alkaline to anorogenic alkaline magmatism. *Bollettino Della Società Geologica Italiana, 2*, 131–152.
Tribuzio, R., Renna, M. R., Braga, R., & Dallai, L. (2009). Petrogenesis of early Permian olivinebearing cumulates and associated basalt dykes from Bocca di Tenda (Northern Corsica): Implications for post-collisional Variscan evolution. *Chemical Geology, 259*, 190–203.
Tribuzio, R., Thirlwall, M. F., & Messiga, B. (1999). Petrology, mineral and isotope geochemistry of the Sondalo gabbroic complex (Central Alps, Northern Italy): implications for the origin of post-Variscan magmatism. *Contributions to Mineralogy and Petrology, 136*(1), 48–62.
Turner, S. P., Platt, J. P., George, R. M. M., Kelley, S. P., Pearson, D. G., & Nowell, G. M. (1999). Magmatism associated with orogenic collapse of the Betic-Alboran domain, SE Spain. *Journal of Petrology, 40*(6), 1011–1036.
Turpin, L., Cuney, M., Friedrich, M., Bouchez, J. L., & Aubertin, M. (1990). Meta-igneous origin of Hercynian peraluminous granites in NW French Massif Central: Implications for crustal history reconstructions. *Contributions to Mineralogy and Petrology, 104*(2), 163–172.
Vavra, G., Schmid, R., & Gebauer, D. (1999). Internal morphology, habit and U-Th-Pb microanalysis of amphibolite-to-granulite facies zircons: Geochronology of the Ivrea Zone (Southern Alps). *Contributions to Mineralogy and Petrology, 134*(4), 380–404.
Veselá, P., Lammerer, B., Wetzel, A., Söllner, F., & Gerdes, A. (2008). Post-Variscan to Early Alpine sedimentary basins in the Tauern window (eastern Alps). *Geological Society, London, Special Publications, 298*(1), 83–100.
Vielzeuf, D., Clemens, J. D., Pin, C., & Moinet, E. (1990). Granites, granulites, and crustal differentiation. In Granulites and crustal evolution (59–85). Springer, Dordrecht.
Vielzuef, D., & Holloway, D. H. (1988). Experimental determination of the fluid-absent melting relations in the pelitic system. *Contributions to Mineralogy and Petrology, 98*, 257–276.
Vielzeuf, D., & Montel, J. M. (1994). Partial melting of metagrey wackes Part I: Fluid-absent experiments and phase relationships. *Contributions to Mineralogy and Petrology, 117*, 375–393.
Visonà, D., Fioretti, A. M., Poli, M. E., Zanferrari, A., & Fanning, M. (2007). U-Pb SHRIMP zircon dating of andesite from the Dolomite area (NE Italy): Geochronological evidence for the early onset of Permian Volcanism in the eastern part of the southern Alps. *Swiss Journal of Geosciences, 100*, 313–324.
von Raumer, J. F. (1998). The Palaeozoic evolution in the Alps: from Gondwana to Pangea. *Geologische Rundschau, 87*(3), 407–435.
Voshage, H., Hofmann, A. W., Mazzucchelli, M., Rivalenti, G., Sinigoi, S., Raczek, I., & Demarchi, G. (1990). Isotopic evidence from the Ivrea Zone for a hybrid lower crust formed by magmatic underplating. *Nature, 347*, 731–736.
Wareham, C. D., Millar, I. L., & Vaughan, A. P. (1997). The generation of sodic granite magmas, western Palmer Land, Antarctic Peninsula. *Contributions to Mineralogy and Petrology, 128*(1), 81–96.
White, A. J., & Chappell, B. W. (1977). Ultrametamorphism and granitoid genesis. *Tectonophysics, 43*(1–2), 7–22.
Whitney, D. L., & Evans, B. W. (2010). Abbreviation of rock-forming minerals. *American Mineralogist, 95*, 185–187.
Willcock, M. A. W., Cas, R. A. F., Giordano, G., & Morelli, C. (2013). The eruption, pyroclastic flow behaviour, and caldera in-filling processes of the extremely large volume (>1290km3), intra- to extra-caldera, Permian Ora (Ignimbrite) Formation, Southern Alps, Italy. *Journal of Volcanology and Geothermal Research, 265*, 102–126.
Wolf, M. B., & Wyllie, P. J. (1989). The formation of tonalitic liquids during the vapor-absent partial melting of amphibolite at 10 kb. *EOS Transactions of the American Geophysical Union, 70*, 506.
Wolf, M. B., & Wyllie, P. J. (1994). Dehydration-melting of amphibolite at 10 kbar: The effects of temperature and time. *Contributions to Mineralogy and Petrology, 115*(4), 369–383.
Woodhead, J. D., Eggins, S. M., & Johnson, R. W. (1998). Magma genesis in the New Britain island arc: Further insights into melting and mass transfer processes. *Journal of Petrology, 39*(9), 1641–1668.
Woodhead, J. D., Hergt, J. M., Davidson, J. P., & Eggins, S. M. (2001). Hafnium isotope evidence for 'conservative'element mobility during subduction zone processes. *Earth and Planetary Science Letters, 192*(3), 331–346.
Wyhlidal, S., Thöny, W. F., Tropper, P., Kaindl, R., Hauzenberger, C., & Mair, V. (2012). Petrology of contact metamorphic metapelites from the southern rim of the Permian Brixen Granodiorite (South Tyrol, Italy). *Mineralogy and Petrology, 106*(3), 173–191.
Zanchetta, S., D'Adda, P., Zanchi, A., Barberini, V., & Villa, I. M. (2011). Cretaceous-Eocene compression in the central Southern Alps (N Italy) inferred from $^{40}Ar/^{39}Ar$ dating of pseudotachylytes along regional thrust faults. *Journal of Geodynamics, 51*, 245–263.
Zanchetta, S., Locchi, S., Carminati, G., Mancuso, M., Montemagni, C., & Zanchi, A. (2022). Metasomatism by Boron-Rich Fluids along Permian Low-Angle Normal Faults (Central Southern Alps, N Italy). *Minerals, 12*(4), 404.
Zanchetta, S., Malusà, M. G., & Zanchi, A. (2015). Precollisional development and Cenozoic evolution of the Southalpine retrobelt (European Alps). *Lithosphere, 7*, 662–681.
Zanchetta, S., Montemagni, C., Mascandola, C., Mair, V., Morelli, C., & Zanchi, A. (2023). The Meran-Mauls Fault: Tectonic switching from compression to transpression along a restraining bend of the Periadriatic Fault. *Journal of Structural Geology*. https://doi.org/10.1016/j.jsg.2023.104878
Zanchi, A., Zanchetta, S., Berio, L., Berra, F., & Felletti, F. (2019). Low-angle normal faults record Early Permian extensional tectonics in the Orobic Basin (Southern Alps, N Italy). *Italian Journal of Geosciences, 138*(2), 184–201.
Zanoni, D., & Spalla, M. I. (2018). The Variscan evolution in the basement cobbles of the Permian Ponteranica Formation by microstructural and petrologic analysis. *Italian Journal of Geosciences, 137*, 254–271.
Zeck, H. P., Kristensen, A. B., & Williams, I. S. (1998). Post-collisional volcanism in a sinking slab setting—crustal anatectic origin of pyroxene-andesite

magma, Caldear Volcanic Group, Neogene Alborán volcanic Province, southeastern Spain. *Lithos, 45*(1–4), 499–522.
Zhang, J. S., Passchier, C. W., Slack, J. F., Fliervoet, T. F., & de Boorder, H. (1994). Cryptocristaline Permian tourmalinites of possible metasomatic origin in the Orobic Alps, northern Italy. *Economic Geology, 89*, 391–396.
Zingg, A., Handy, M. R., Hunziker, J. C., & Schmid, S. M. (1990). Tectonometamorphic history of the Ivrea Zone and its relationship to the crustal evolution of the Southern Alps. *Tectonophysics, 182*(1–2), 169–192.

Publisher's Note